

# Contents

## *Chapter 1*

### **FUNDAMENTALS OF PLASMA CHEMISTRY** 1

Alexis T. Bell

## *Chapter 2*

### **APPLICATIONS OF NONEQUILIBRIUM PLASMAS TO ORGANIC CHEMISTRY** 57

Harald Suhr

## *Chapter 3*

### **PLASMA TREATMENT OF SOLID MATERIALS** 113

Martin Hudis

## *Chapter 4*

### **PLASMA TREATMENT OF NATURAL MATERIALS** 149

Attila E. Pavlath

## *Chapter 5*

### **SYNTHESIS OF ORGANIC POLYMER FILMS IN PLASMAS** 177

Merle Millard

## *Chapter 6*

### **SEMIPERMEABLE MEMBRANES PRODUCED BY PLASMA POLYMERIZATION** 215

Theodore Wydeven and John R. Hollahan

*Chapter 7*

<b>APPLICATIONS OF LOW-TEMPERATURE PLASMAS TO CHEMICAL AND PHYSICAL ANALYSIS</b>	<b>229</b>
--	------------

John R. Hollahan

*Chapter 8*

<b>USE OF CHEMICALLY REACTIVE GASEOUS PLASMAS IN PREPARATION OF SPECIMENS FOR MICROSCOPY</b>	<b>255</b>
--	------------

Richard S. Thomas

*Chapter 9*

<b>APPLICATIONS OF PLASMA TECHNOLOGY TO THE FABRICATION OF SEMICONDUCTOR DEVICES</b>	<b>347</b>
--	------------

Ralph W. Kirk

*Chapter 10*

<b>ENGINEERING AND ECONOMIC ASPECTS OF PLASMA CHEMISTRY</b>	<b>379</b>
---	------------

Alexis T. Bell

*Appendix*

<b>DESIGN OF RADIO-FREQUENCY EQUIPMENT USED TO SUSTAIN ELECTRIC DISCHARGES</b>	<b>393</b>
--	------------

<b>INDEX</b>	<b>401</b>
--------------	------------

**Techniques  
and Applications of  
Plasma Chemistry**

# Fundamentals of Plasma Chemistry

Alexis T. Bell

1.1. INTRODUCTION	1
1.2. PLASMA KINETIC THEORY	3
Electron-Velocity Distribution Functions	3
The Boltzmann Equation	5
Solutions to the Boltzmann Equation	6
1.3. TRANSPORT PHENOMENA	15
Electron-Transport Properties	15
Energy Transfer	19
Diffusion of Charged Species	20
1.4. CHEMICAL REACTIONS OCCURRING IN PLASMAS	26
1.5. PHYSICAL CHARACTERISTICS OF HIGH-FREQUENCY DISCHARGES	35
Breakdown and Steady-State Operating Conditions	35
Electric Field and Electron-Density Distributions	40
1.6. PRODUCTION OF ATOMIC OXYGEN IN A MICROWAVE DISCHARGE	45
REFERENCES	55

## 1.1. INTRODUCTION

The field of plasma chemistry deals with the occurrence of chemical reactions in a partially ionized gas composed of ions, electrons, and neutral species. This state of matter can be produced through the action of either very high temperatures or strong electric or magnetic fields. The present book focuses attention on ionized gas produced by gaseous electric discharges. In a discharge, free electrons gain energy from an imposed electric field and lose this energy through collisions with neutral gas molecules. The transfer of energy to the molecules leads to the formation of a variety of new species including metastables, atoms, free radicals, and ions. These products are all active chemically and thus can serve as precursors to the formation of new stable compounds.

## 2 FUNDAMENTALS OF PLASMA CHEMISTRY

For the ionized gas produced in a discharge to be properly termed a plasma, it must satisfy the requirement that the concentrations of positive and negative charge carriers are approximately equal. This criterion is satisfied when the dimensions of the discharged gas volume characterized by  $\Lambda$  are significantly larger than the Debye length

$$\lambda_D = \left( \frac{\epsilon_0 k T_e}{n e^2} \right)^{1/2} \quad (1.1)$$

which defines the distance over which a charge imbalance can exist. In (1.1)  $\epsilon_0$  is the permittivity of free space,  $k$  is the Boltzmann constant,  $T_e$  is the electron temperature,  $n$  is the electron density, and  $e$  is the charge on the electron.

Many types of electric discharge have been described in the physical literature and the properties of the plasma produced in them can differ widely. Figure 1.1 illustrates the characteristics for a number of man-made as well as naturally occurring plasmas in terms of the electron temperature and density. The two regions of greatest interest to plasma chemistry are

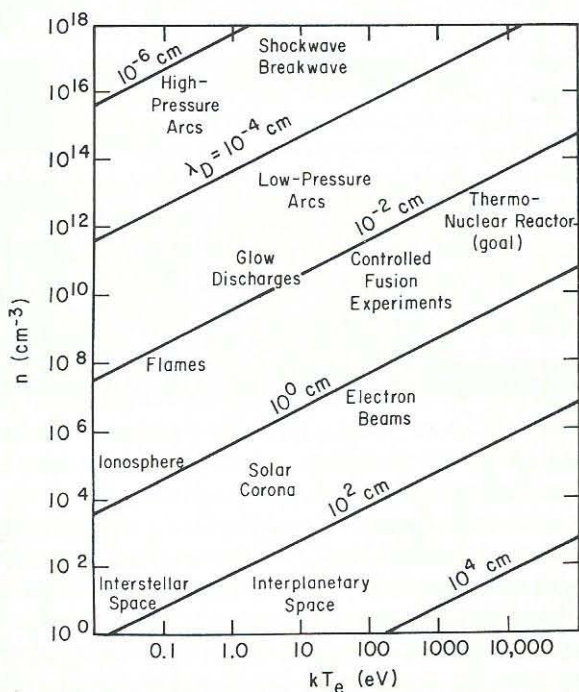


FIGURE 1.1. Typical plasmas characterized by their electron energy and density.

those labeled "glow discharges" and "arcs." The plasma produced in a glow discharge is characterized by average electron energies of 1–10 eV and electron densities of  $10^9$ – $10^{12}$   $\text{cm}^{-3}$ . An additional characteristic of such plasmas is the lack of equilibrium between the electron temperature  $T_e$  and the gas temperature  $T_g$ . Typical ratios for  $T_e/T_g$  lie in the range of 10– $10^2$ . The absence of thermal equilibrium makes it possible to obtain a plasma in which the gas temperature may be near ambient values at the same time that the electrons are sufficiently energetic to cause the rupture of molecular bonds. [It is this characteristic which makes glow-discharge plasmas well suited for the promotion of chemical reactions involving thermally sensitive materials.]

By contrast, the conditions found in the plasmas produced by arcs or plasma jets lead to an equilibrium situation in which the electron and gas temperatures are nearly identical. The very high gas temperatures ( $>5 \times 10^3$  °K) measured in arcs and plasma jets makes them suitable for processing inorganic materials and organic compounds with very simple structures. More complex organic materials and polymers cannot be treated under these conditions since they would be rapidly degraded.

Since the applications described in this book deal exclusively with plasmas produced in glow discharges, the balance of this chapter will be devoted to a discussion of their physical and chemical properties. This discussion will begin with an examination of the factors controlling the electron-velocity distribution and in turn the average electron energy. The determination of the plasma transport properties are discussed next. This is followed by an examination of the types of chemical reactions which occur in plasmas and the means available for describing their kinetics. The material of the previous sections is then brought together to give a complete physical characterization of the plasma as a function of its operating conditions. Finally, using the dissociation of oxygen as an example, a model of the reaction kinetics in a discharge is assembled and tested against experimental data.

## 1.2. PLASMA KINETIC THEORY

### Electron-Velocity Distribution Functions

The electron-velocity distribution plays a central role in defining the physical properties of a plasma. From it are derived the electron-energy distribution, the average electron energy, the electron-transport properties, and the rate constants for reactions involving electron-molecule collisions. As we shall see from the development presented below, the shape of the distribution function depends upon the magnitude of the applied electric field and the nature of the elastic and inelastic interactions which the electrons undergo.

#### 4 FUNDAMENTALS OF PLASMA CHEMISTRY

By definition, the electron-velocity distribution function  $f$  represents the density of electrons in both position and velocity space. If the vector  $\mathbf{r}$  is used to describe a given point in position space and the vector  $\mathbf{v}$  a given point in velocity space,  $f$  may be expressed as  $f(\mathbf{r}, \mathbf{v})$ . The product  $f d\mathbf{r} d\mathbf{v}$ , in which  $d\mathbf{r} = dx dy dz$  and  $d\mathbf{v} = dv_x dv_y dv_z$ , denotes the number of electrons whose positions are located within the volume element  $d\mathbf{r}$  and whose velocities lie within the volume element  $d\mathbf{v}$ . Dividing  $f d\mathbf{r} d\mathbf{v}$  by  $d\mathbf{r}$  gives us  $f d\mathbf{v}$ , the number of electrons per unit volume at  $\mathbf{r}$  with velocities in  $d\mathbf{v}$ . If the product  $f d\mathbf{v}$  is integrated, we will obtain the electron density at the point  $\mathbf{r}$ . Thus

$$n = \int_{-\infty}^{\infty} f d\mathbf{v} \quad (1.2)$$

where the single integral sign is used to denote a triple integration extending over the three coordinates of velocity space.

If  $\phi(\mathbf{r}, \mathbf{v})$  defines some property of the electrons which might depend on both position and velocity, the average value of this property weighted against the distribution of velocities can be expressed as

$$n\langle\phi\rangle = \int_{-\infty}^{\infty} \phi f d\mathbf{v} \quad (1.3)$$

Thus, for instance, to evaluate the average translational velocity  $\langle v_x \rangle$ , let  $\phi = v_x$ . Then

$$\langle v_x \rangle = \frac{1}{n} \int_{-\infty}^{\infty} v_x f d\mathbf{v} \quad (1.4)$$

Equation (1.3) can also be used to determine the average electron energy. We begin by noting that the velocity  $\mathbf{v}$  can be expressed as  $\mathbf{v} = \mathbf{V} + \langle \mathbf{v} \rangle$ , the sum of the random velocity plus the translational velocity of the whole electron cloud. Since positive and negative values of  $\mathbf{V}$  are equally probable, the average value of  $\mathbf{V}$  will equal zero. The total translational kinetic energy can then be expressed as

$$\begin{aligned} \varepsilon = \frac{1}{2}m\langle v^2 \rangle &= \frac{1}{n} \int_{-\infty}^{\infty} \frac{1}{2}m\mathbf{v} \cdot \mathbf{v} f d\mathbf{v} \\ &= \frac{1}{2}m\langle (\mathbf{V} + \langle \mathbf{v} \rangle) \cdot (\mathbf{V} + \langle \mathbf{v} \rangle) \rangle \\ &= \frac{1}{2}m(\langle \mathbf{V} \cdot \mathbf{V} \rangle + 2\langle \mathbf{V} \rangle \cdot \langle \mathbf{v} \rangle + \langle \mathbf{v} \rangle \cdot \langle \mathbf{v} \rangle) \\ &= \frac{1}{2}m\langle V^2 \rangle + \frac{1}{2}m\langle v \rangle^2 \end{aligned} \quad (1.5)$$

where  $v$  and  $V$  are the magnitudes of the velocities  $\mathbf{v}$  and  $\mathbf{V}$ , respectively. The first term in (1.5) represents the kinetic energy associated with the random motion of the electrons, and the second term represents the kinetic energy associated with the translation of the electron cloud as a whole. In a system in which the velocity distribution is Maxwellian, the random kinetic energy can be related to the electron temperature by

$$\frac{1}{2}m\langle V^2 \rangle = \frac{3}{2}kT_e \quad (1.6)$$

### The Boltzmann Equation

The exact form of the velocity distribution function can be derived through consideration of the gain and loss of electrons from an incremental volume in phase space defined by  $d\mathbf{r} d\mathbf{v}$ . The equation summarizing the net rate of transfer of electrons from this volume is known as the Boltzmann equation and is expressed as

$$\frac{\partial f}{\partial t} + \mathbf{v} \cdot \nabla_{\mathbf{r}} f + \frac{e\mathbf{E}}{m} \cdot \nabla_{\mathbf{v}} f = \left( \frac{\partial f}{\partial t} \right)_{\text{coll}} \quad (1.7)$$

The first term on the left-hand side of (1.7) gives the local variation of the distribution function with time. The second term describes the variation in the distribution function resulting from electrons streaming in and out of a given volume element. This term is closely related to the description of diffusion. The third term is the variation of the distribution function resulting from an applied electric field  $\mathbf{E}$  acting on the electrons. The single term on the right-hand side of (1.7) accounts for the net transfer of electrons from the differential volume by the mechanism of binary collisions between electrons and molecules, ions, and other electrons.

The net rate at which electrons are removed from the differential volume  $d\mathbf{v}$  by binary collisions is given by

$$\left( \frac{\partial f}{\partial t} \right)_{\text{coll}} = \int_{-\infty}^{\infty} \int_0^{\pi} (\tilde{f}\tilde{f}_T - ff_T) g \sigma(\chi, v) 2\pi \sin \chi d\chi dv_T \quad (1.8)$$

In this expression  $f$  and  $f_T$  are the velocity distribution functions of the electrons and target particles, respectively;  $g$  is the relative velocity; and  $\sigma(\chi, v)$  is the collision cross-section which depends on the scattering angle  $\chi$  and the electron speed  $v$ . The second term on the right-hand side of (1.8) describes the rate at which electrons are removed from  $d\mathbf{v}$  by collisions. The product  $\tilde{f}\tilde{f}_T$  associated with this term is evaluated at the velocities  $v$  and  $v_T$  which hold just before collision. The first term on the right-hand side of

## 6 FUNDAMENTALS OF PLASMA CHEMISTRY

(1.8) describes the rate at which electrons are scattered into  $d\mathbf{v}$  by collisions which are the reverse of those removing electrons from  $d\mathbf{v}$ . In this case the product  $\tilde{f}\tilde{f}_T$  must be evaluated at the velocities  $\tilde{v}$  and  $\tilde{v}_T$  which describe the motion of the electron and target immediately after collision. The two sets of velocities are related to each other by the conservation of momentum and energy.

Many types of binary collisions can occur within a plasma. These can most conveniently be broken down into the categories of elastic and inelastic collisions. The former involves electron collisions with either neutral or charged targets such that there is no excitation of the target particle. If the target is a molecule or ion, then there is only a very small transfer of energy from the electrons. By contrast, interactions between two electrons can lead to a significant transfer of energy from one electron to another and, as we shall see, play an important role in shaping the electron-velocity distribution function. Inelastic collisions differ from elastic collisions in that the target particle is left in an excited state after collision. The nature of these excitations ranges across the energy spectrum from rotational excitations in which 0.01–0.1 eV is absorbed to ionizations in which more than 10 eV is absorbed.

### Solutions to the Boltzmann Equation

The Boltzmann equation must be solved in order to obtain the velocity distribution function. Since no exact solution to this equation is known, an approximate solution must be sought. A technique which has been used extensively considers that the solution can be expressed as the sum of an isotropic portion plus a small anisotropic perturbation. The basis for this form is the observation that, in the absence of any fields or gradients in electron concentration, the velocity distribution becomes completely isotropic. The effect of spatial gradients and external forces is thus assumed to produce a perturbation onto the isotropic solution. Under this assumption, the distribution function  $f$  can be expressed as

$$f = f^\circ + \phi(\mathbf{v}) \quad (1.9)$$

where  $f^\circ$  is the isotropic distribution and  $\phi(\mathbf{v})$  the anisotropic distribution. It may be further assumed that the anisotropic contribution is largest when  $\mathbf{v}$  is in the direction of the gradient or force causing the perturbation and smallest when it is perpendicular to it. By this reasoning we can express the anisotropic distribution as

$$\phi(\mathbf{v}) = \frac{\mathbf{v}}{v} \cdot \mathbf{f}' \quad (1.10)$$

in which the vector  $\mathbf{f}'$  points in the direction in which the electrons drift as the result of the external fields and spatial gradients. The total distribution can then be written as

$$f = f^\circ + \frac{\mathbf{v}}{v} \cdot \mathbf{f}' \quad (1.11)$$

Substitution of the approximate solution (1.11) into the Boltzmann equation leads to the identification of two differential equations which can be solved for  $f^\circ$  and  $\mathbf{f}'$ . The procedure by which this is accomplished is quite complex and it is suggested that the reader who is interested in the details consult the discussion of this problem given by Allis [1]. The two equations which are the final result can be expressed as

$$\frac{\partial f^\circ}{\partial t} + \frac{v}{3} \nabla_r \cdot \mathbf{f}' - \frac{e\mathbf{E}}{3mv^2} \cdot \frac{\partial}{\partial v} (v^2 \mathbf{f}') = \left( \frac{\partial f^\circ}{\partial t} \right)_{cc} + \left( \frac{\partial f^\circ}{\partial t} \right)_{cm} + \left( \frac{\partial f^\circ}{\partial t} \right)_{cx} \quad (1.12)$$

$$\frac{\partial \mathbf{f}'}{\partial t} + v \nabla_r f^\circ - \frac{e\mathbf{E}}{m} \frac{\partial f^\circ}{\partial v} = \left( \frac{\partial \mathbf{f}'}{\partial t} \right)_{cc} + \left( \frac{\partial \mathbf{f}'}{\partial t} \right)_{cm} + \left( \frac{\partial \mathbf{f}'}{\partial t} \right)_{cx} \quad (1.13)$$

The three terms appearing on the right-hand side of these equations describe the effects of coulombic, elastic, and inelastic collisions, respectively.

The elastic collision contributions to the right-hand sides of (1.12) and (1.13) are given by

$$\left( \frac{\partial f^\circ}{\partial t} \right)_{cm} = \frac{m}{M} \frac{1}{v^2} \frac{\partial}{\partial v} (v_m v^3 f^\circ) + \frac{1}{v^2} \frac{\partial}{\partial v} \left( v_m v^2 \frac{kT_g}{M} \frac{\partial f^\circ}{\partial v} \right) \quad (1.14)$$

$$\left( \frac{\partial \mathbf{f}'}{\partial t} \right)_{cm} = -v_m \mathbf{f}' \quad (1.15)$$

where  $m$  and  $M$  are the mass of the electron and target molecule, respectively. The momentum transfer collision frequency  $\nu_m$  is defined by

$$\nu_m = 2\pi N v \int_0^\pi (1 - \cos \chi) \sigma_e(\chi, v) \sin \chi \, d\chi \quad (1.16)$$

in which  $N$  is the total gas density and  $\sigma_e$  is the elastic collision cross-section.

Inelastic collisions contribute principally to the distribution of velocities and relatively little to the transport properties associated with the electrons. As a result, the appropriate terms appearing in (1.12) and (1.13) will be

given by

$$\left(\frac{\partial f^{\circ}}{\partial t}\right)_{cx} = \sum_i \left(\frac{\tilde{v}}{v} \tilde{f}^{\circ}(\tilde{v}) \nu_i(\tilde{v}) - f^{\circ}(v) \nu_i(v)\right) \quad (1.17)$$

$$\left(\frac{\partial \mathbf{f}'}{\partial t}\right)_{cx} = 0 \quad (1.18)$$

where  $1/2 mv^2 = 1/2 m\tilde{v}^2 + \varepsilon_i$ . The collision frequency  $\nu_i$  for each inelastic process is related to the cross-section for that process by

$$\nu_i = Nv\sigma_i(v) \quad (1.19)$$

The physical significance of the two terms appearing in (1.17) will be discussed below.

Coulombic collisions arising from the interaction of electrons with either ions or other electrons become significant only when the fractional degree of ionization is substantial [2]. In most high-frequency glow discharges, the degree of ionization is small enough ( $<10^{-5}$ ) for coulombic collisions to be neglected. Thus the terms  $(\partial f^{\circ}/\partial t)_{cc}$  and  $(\partial \mathbf{f}'/\partial t)_{cc}$  appearing in (1.12) and (1.13) may be set equal to zero.

The final form of (1.12) and (1.13) can be obtained by introducing the expressions for the collision terms. Thus

$$\begin{aligned} \frac{\partial f^{\circ}}{\partial t} + \frac{v}{3} \nabla_r \cdot \mathbf{f}' - \frac{e\mathbf{E}}{3mv^2} \cdot \frac{\partial}{\partial v} (v^2 \mathbf{f}') \\ = \frac{m}{M} \frac{1}{v^2} \frac{\partial}{\partial v} \left( \nu_m v^3 f^{\circ} + \frac{\nu_m k T_g}{m} v^2 \frac{\partial f^{\circ}}{\partial v} \right) + \sum_i \left( \frac{\tilde{v}}{v} \tilde{f}^{\circ} \tilde{\nu}_i - f^{\circ} \nu_i \right) \end{aligned} \quad (1.20)$$

$$\frac{\partial \mathbf{f}'}{\partial t} + v \nabla_r f^{\circ} - \frac{e}{m} \mathbf{E} \frac{\partial f^{\circ}}{\partial v} = -\nu_m \mathbf{f}' \quad (1.21)$$

The solution of these two equations for  $f^{\circ}$  and  $\mathbf{f}'$  will now be illustrated by several simple examples.

Consider a homogeneous, isotropic plasma in the presence of an alternating electric field  $\mathbf{E}_0 e^{-i\omega t}$ . Then, assuming that the time dependence of  $\mathbf{f}'$  is given by  $e^{-i\omega t}$ , the solution for  $\mathbf{f}'$  may be obtained from (1.21) as

$$\mathbf{f}' = \frac{e\mathbf{E}}{m(\nu_m - i\omega)} \frac{\partial f^{\circ}}{\partial v} \quad (1.22)$$

Neglecting spatial gradients, (1.20) can be written as

$$\frac{e\mathbf{E}}{3mv^2} \cdot \frac{\partial}{\partial v} (v^2 \mathbf{f}') + \frac{m}{M} \frac{1}{v^2} \frac{\partial}{\partial v} \left( v_m v^3 f^\circ + \frac{v_m k T_g}{m} v^2 \frac{\partial f^\circ}{\partial v} \right) + \sum_i \left( \frac{\tilde{v}}{v} \tilde{f}^\circ \tilde{v}_i - f^\circ v_i \right) = 0 \quad (1.23)$$

The time dependence of  $f^\circ$  has been neglected in (1.23) since it has been shown by Margenau [3] that it is small in comparison to the steady-state value of  $f^\circ$  for  $\omega \gg (2m/M)v_m$ .

Introduction of the solution for  $\mathbf{f}'$  into (1.23) requires that the product  $\mathbf{E} \cdot \mathbf{f}'$  be interpreted as the time average of the product of the real parts of  $\mathbf{E}$  and  $\mathbf{f}'$ . With this interpretation, (1.23) can be rewritten as

$$\frac{1}{2v^2} \frac{\partial}{\partial v} \left[ \frac{e^2 E_0^2 v_m v^2}{3m^2 (v_m^2 + \omega^2)} \frac{\partial f^\circ}{\partial v} + \frac{2m}{M} v_m v^2 \left( v f^\circ + \frac{k T_g}{M} \frac{\partial f^\circ}{\partial v} \right) \right] + \sum_i \left( \frac{\tilde{v}}{v} \tilde{f}^\circ \tilde{v}_i - f^\circ v_i \right) = 0 \quad (1.24)$$

It should be noted that (1.24) could also have been obtained for the case of a dc field with the exception that  $E_0^2 v_m^2 / 2(v_m^2 + \omega^2)$  appearing in the first term would have been replaced by  $E_{dc}^2$ . If we define an effective field  $E_e$  by  $E_0 \sqrt{v_m^2 / 2(v_m^2 + \omega^2)}$ , then identical distribution functions will result when  $E_e = E_{dc}$ .

The physical significance of (1.24) can be illustrated if we multiply each term by  $1/2 mv^2$  and integrate over all speeds. Thus

$$\begin{aligned} & \frac{(eE_e)^2}{m v_m} \int_0^\infty f^\circ 4\pi v^2 dv \\ &= \frac{2m}{M} v_m \int_0^\infty \frac{mv^2}{2} f^\circ 4\pi v^2 dv - \frac{2m}{M} \frac{3kT_g}{2} v_m \int_0^\infty f^\circ 4\pi v^2 dv \\ & \quad - \sum_i \int_0^\infty \left( \frac{\tilde{v}}{v} \tilde{f}^\circ \tilde{v}_i - f^\circ v_i \right) \frac{mv^2}{2} 4\pi v^2 dv \end{aligned} \quad (1.25)$$

where, for the sake of simplicity,  $v_m$  is assumed to be independent of  $v$ . The left-hand side of (1.25) represents the rate at which energy is transferred from the electric field to the electrons. The first term on the right-hand side gives the rate at which the electrons lose energy by elastic collisions. The second term gives the energy gained by slow electrons colliding with faster

## 10 FUNDAMENTALS OF PLASMA CHEMISTRY

moving molecules. The final term represents the net loss of energy due to inelastic collisions.

If the value of  $E_0$  is set to zero and we neglect inelastic losses, (1.24) reduces to

$$vf^\circ + \frac{kT_g}{m} \frac{\partial f^\circ}{\partial v} = 0 \quad (1.26)$$

For this case  $f^\circ$  is given by

$$f^\circ = Ce^{-mv^2/2kT_g} \quad (1.27)$$

and is therefore Maxwellian. Under these conditions the electrons are in equilibrium with the gas molecules and are characterized by the gas temperature  $T_g$ .

At low electric field strengths, the loss of energy by inelastic collisions will be negligible since very few electrons will possess sufficient energy to bring about such excitations. Under these conditions (1.24) takes the form

$$\frac{1}{v^2} \frac{\partial}{\partial v} \left[ \frac{e^2 E_e^2 v^2}{3m^2 \nu_m} \frac{\partial f^\circ}{\partial v} + \frac{m}{M} v^2 \nu_m \left( vf^\circ + \frac{kT_g}{m} \frac{\partial f^\circ}{\partial v} \right) \right] = 0 \quad (1.28)$$

Integrating once, we obtain

$$v^2 \left[ \frac{e^2 E_e^2}{3m^2 \nu_m} \frac{\partial f^\circ}{\partial v} + \frac{m}{M} \nu_m \left( vf^\circ + \frac{kT_g}{m} \frac{\partial f^\circ}{\partial v} \right) \right] = 0 \quad (1.29)$$

where the constant of integration is zero since  $f^\circ$  must be Maxwellian when  $E_e = 0$ .

Equation (1.29) can be rewritten as

$$\frac{\partial f^\circ}{\partial v} \left( \frac{e^2 E_e^2 M}{3m^2 \nu_m^2} + kT_g \right) + mvf^\circ = 0 \quad (1.30)$$

The solution of (1.30) is then

$$f^\circ = C \exp - \left( \int_0^v \frac{mv \, dv}{kT_g + e^2 E_e^2 M / 3m^2 \nu_m^2} \right) \quad (1.31)$$

where the constant  $C$  is determined by the normalization condition

$$n = 4\pi \int_0^\infty f^\circ v^2 \, dv \quad (1.32)$$

The form of  $f^\circ$  given by (1.31) is known as the Margenau distribution.

We may now consider the case in which the applied electric field is sufficiently large to cause the second term in the denominator of the integral appearing in (1.31) to be much greater than  $kT_g$ . In addition, we will assume a sufficiently low frequency for the applied field such that  $\omega^2 \ll \nu^2$ . The Margenau distribution can then be approximated as

$$f^\circ = C \exp - \left( \int_0^v \frac{mv \, dv}{e^2 E_0^2 M / 6m^2 \nu_m^2} \right) \quad (1.33)$$

The integral appearing in (1.33) can be evaluated in closed form provided we make some assumptions concerning the dependence of  $\nu_m$  on velocity. From the kinetic theory  $\nu_m(v)$  can be expressed as

$$\nu_m = Nv\sigma_m(v) \quad (1.34)$$

where  $\sigma_m$  is the momentum collision cross-section. For certain gases such as helium and hydrogen  $\sigma_m(v)$  is found to vary as  $1/v$ , and, for such gases, the momentum collision frequency is therefore independent of velocity. In these cases the Margenau distribution will be given by

$$f^\circ = C \exp - \left( \frac{mv^2/2}{e^2 E_0^2 M / 6m^2 \nu_m^2} \right) \quad (1.35)$$

Equation (1.35) has the same form as a Maxwellian distribution in which

$$kT_e = \frac{e^2 E_0^2 M}{6m^2 \nu_m^2} \quad (1.36)$$

When the collision cross-section is independent of velocity, the collision frequency  $\nu_m$  becomes a linear function of velocity. Under such conditions the Margenau distribution may be expressed as

$$\begin{aligned} f^\circ &= C \exp - \left( \int_0^v \frac{6m^3 N^2 \sigma_m^2 v^3 \, dv}{e^2 E_0^2 M} \right) \\ &= C \exp - \left[ \frac{(mv^2/2)^2}{e^2 E_0^2 M / 6m N^2 \sigma_m^2} \right] \end{aligned} \quad (1.37)$$

Equation (1.37) is known as the Druyvesteyn distribution. Since the Druyvesteyn distribution varies as  $e^{-av^4}$ , the tail of this distribution decreases more rapidly than the Maxwellian distribution. Figure 1.2 shows that, for a

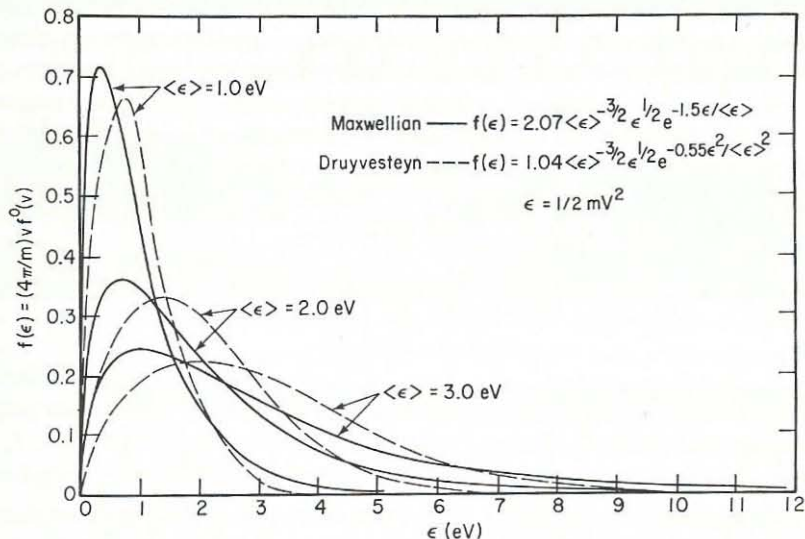


FIGURE 1.2. Comparison of Maxwellian and Druyvesteyn energy distribution functions.

plasma with a given mean energy, the Druyvesteyn distribution predicts fewer high-energy electrons than does the Maxwellian distribution.

An important conclusion which can be derived from (1.36) is that the average electron energy expressed in terms of  $T_e$  is a function solely of  $E_0/p$ . This result comes about from the linear dependence of  $\nu_m$  on pressure. A similar conclusion can be drawn for the Druyvesteyn distribution. There it may be noted that the denominator in the exponential portion of (1.37) represents the square of the average electron energy. Since the gas density  $N$  is proportional to pressure, the average electron energy is again seen to be a function solely of  $E_0/p$ . The effects of electron density on the average electron energy are absent in the two cases examined here. However, as will be discussed below the electron density can have an effect when the fractional degree of ionization becomes large.

The Margenau and Druyvesteyn distributions provide valid solutions to the Boltzmann equation for electric field strengths which are sufficiently low to allow the neglect of inelastic collisions. These conditions are rarely valid in a steady-state discharge. As a result we must return to (1.24) and examine its solution in the presence of inelastic collisions. Since the form of (1.24) becomes quite complex in this case, it is not feasible to provide an analytic solution and one must turn to numerical methods.

An interesting example of the solution of the Boltzmann equation is discussed by Dreicer [2]. In this work the electron-velocity distribution is

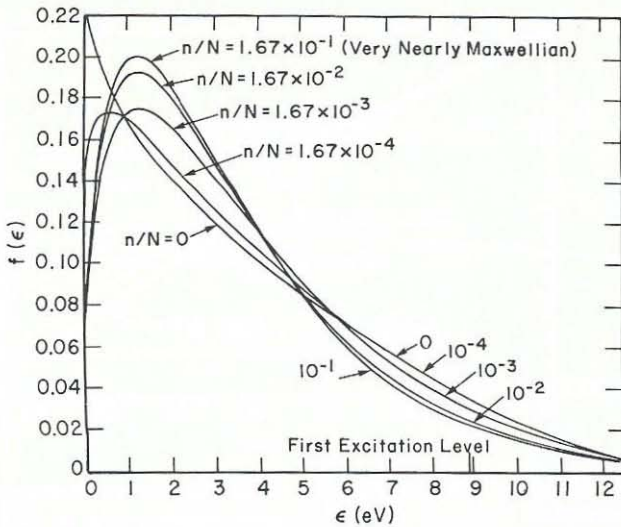


FIGURE 1.3. Effect of the extent of ionization on the energy distribution function for a hydrogen plasma;  $E/p$  is held constant at 28.3 V/cm torr [2].

calculated for a hydrogen plasma, taking into account inelastic collisions as well as random two-body coulombic collisions. Elastic collisions between electrons and hydrogen molecules are neglected on the basis that they represent only a small energy loss term. In consideration of the coulombic interactions only those occurring between two electrons are retained since it is shown that electron-ion encounters result in negligible energy losses from the electron.

Figures 1.3–1.5 illustrate the numerical solutions obtained for  $E/p$  equal to 28.3 V/cm torr and 48.9 V/cm torr. The function plotted on the ordinate is electron-energy distribution function which is related to the velocity distribution function by

$$f(\varepsilon) = \frac{4\pi}{m} v f^\circ(v) \quad (1.38)$$

where  $\varepsilon = 1/2 mv^2$ . For each value of  $E/p$ , the effects of the extent of ionization are identified by the value of  $n/N$ . At very low energies  $f(\varepsilon)$  decreases as the extent of ionization increases. In the neighborhood of 1 eV, the distributions cross each other and the situation is reversed. At still higher energies, the distributions cross each other two more times until in the very high-energy tail we find the population increasing with degree of ionization. It should be noted that at the highest degree of ionization the distribution function is very nearly Maxwellian.

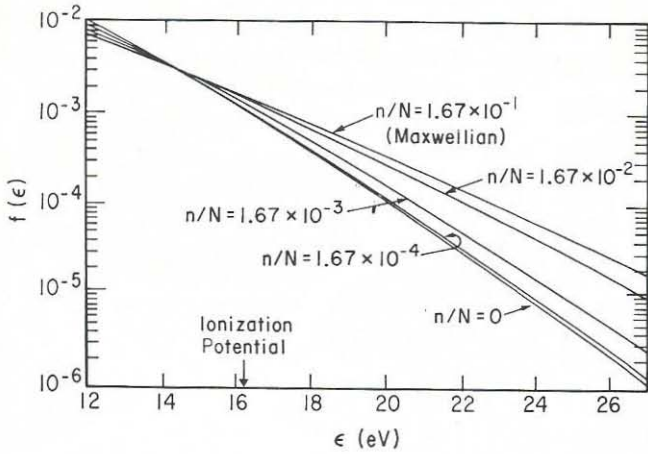


**FIGURE 1.4.** Effect of the extent of ionization on the energy distribution function for a hydrogen plasma;  $E/p$  is held constant at 28.3 V/cm torr [2].

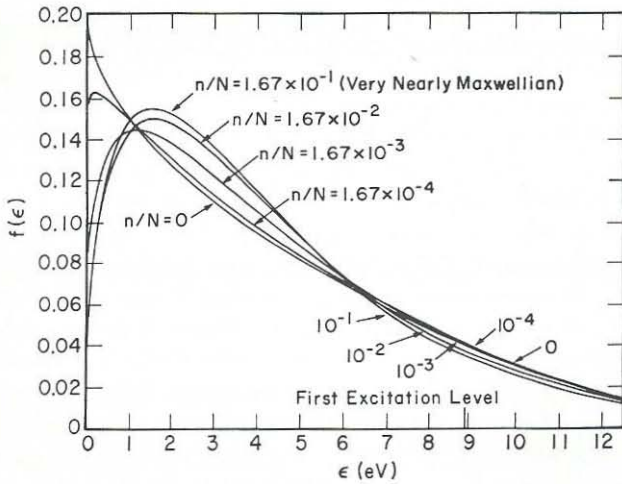


**FIGURE 1.5.** Effect of the extent of ionization on the energy distribution function for a hydrogen plasma;  $E/p$  is held constant at 48.9 V/cm torr [2].

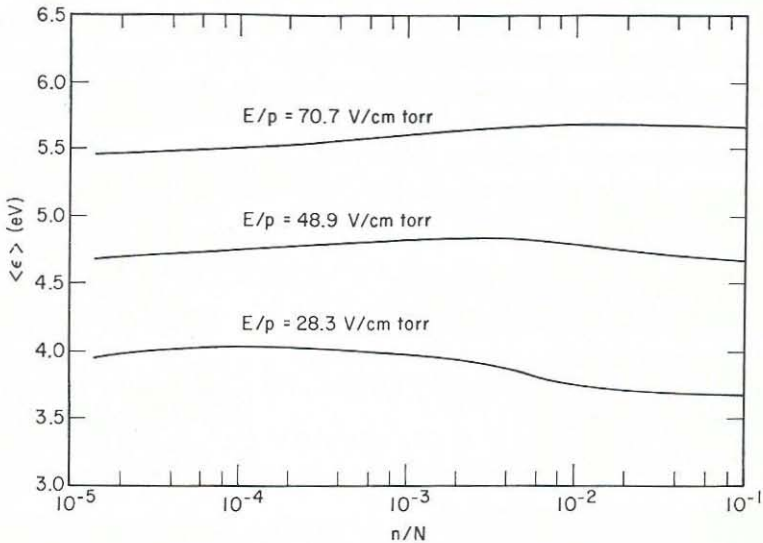


FIGURE 1.6. Variation of the average electron energy with the extent of ionization [2].

The effects of electron interactions on the average energy are illustrated in Figure 1.6. As the degree of ionization increases, the average energy first rises and then falls. The rise is attributed to the fact that the slow electrons produced in inelastic encounters exchange energy with other electrons, and are quickly redistributed over the body of the distribution. For a fixed value of  $E/p$  and  $N$ , the rise in average energy is accomplished by the addition to the distribution of electrons whose average energy exceeds the average energy corresponding to  $n/N = 0$ . The subsequent fall in average energy as  $n/N$  increases even further reflects the fact that coulomb encounters have decreased the population in the neighborhood of the first excitation potential and have redistributed these electrons primarily into lower energy regions. A small number of electrons are also redistributed into the very high-energy tail of the distribution. Ultimately, when  $n/N$  becomes large enough so that the rate at which electrons exchange energy with each other greatly exceeds the rate at which they gain energy from the field, the distribution function becomes Maxwellian.

### 1.3. TRANSPORT PHENOMENA

#### Electron-Transport Properties

The electron-velocity distribution discussed in the previous section can be used to evaluate the transport properties of electrons. In this section we shall

## 16 FUNDAMENTALS OF PLASMA CHEMISTRY

focus on the development of expressions for the electron conductivity and diffusivity. These properties will then be used to determine the spatial distribution of charged particles in a plasma and the rate at which energy is transferred from the sustaining electric field.

A common starting point for the evaluation of both electron conductivity and diffusivity is the flux vector  $\mathbf{\Gamma}$  given by

$$\mathbf{\Gamma} = n\langle \mathbf{v} \rangle = \int_{-\infty}^{\infty} \mathbf{v} f d\mathbf{v} \quad (1.39)$$

The volume element  $d\mathbf{v}$  expressed in spherical coordinates is

$$d\mathbf{v} = v^2 \sin \theta d\theta d\phi dv \quad (1.40)$$

Substituting (1.11) and (1.40) into (1.39), we obtain

$$\mathbf{\Gamma} = \int_0^{\infty} \int_0^{2\pi} \int_0^{\pi} \mathbf{v} f^{\circ} v^2 \sin \theta d\theta d\phi dv + \int_0^{\infty} \int_0^{2\pi} \int_0^{\pi} \mathbf{v}(\mathbf{v} \cdot \mathbf{f}') v \sin \theta d\theta d\phi dv \quad (1.41)$$

Since  $f^{\circ}$  is isotropic and a function of  $v$  alone, the integral over  $v$  causes the first term in (1.41) to vanish. The second term can be simplified by taking into account the properties of spherical coordinates. By this means  $\mathbf{\Gamma}$  becomes

$$\mathbf{\Gamma} = \frac{4}{3}\pi \int_0^{\infty} \mathbf{f}' v^3 dv \quad (1.42)$$

From (1.42) we thus see that  $\mathbf{\Gamma}$  depends on  $\mathbf{f}'$  alone. However, since  $\mathbf{f}'$  and  $f^{\circ}$  are related,  $\mathbf{\Gamma}$  will depend on  $f^{\circ}$  indirectly.

The conductivity of a plasma placed in a uniform ac electric field can be evaluated from (1.42). From the previous section we have seen that the anisotropic portion of the velocity distribution is given by

$$\mathbf{f}' = \frac{e\mathbf{E} \partial f^{\circ} / \partial v}{m(\nu_m - i\omega)} \quad (1.43)$$

for these conditions. Making use of this result we can express the current

density in the plasma as

$$\begin{aligned}
 \mathbf{J} &= -e\mathbf{\Gamma} \\
 &= -\frac{4}{3}e\pi \int_0^\infty \mathbf{f}'v^3 dv \\
 &= -\frac{4\pi e^2}{3m} \mathbf{E} \int_0^\infty \frac{v^3}{(\nu_m - i\omega)} \frac{\partial f^\circ}{\partial v} dv \\
 &= \sigma \mathbf{E}
 \end{aligned} \tag{1.44}$$

Hence the conductivity is defined by

$$\sigma = -\frac{4\pi e^2}{3m} \int_0^\infty \frac{v^3}{(\nu_m - i\omega)} \frac{\partial f^\circ}{\partial v} dv \tag{1.45}$$

If it is assumed that  $f^\circ$  is Maxwellian, then

$$f^\circ = n \left( \frac{m}{2\pi kT_e} \right)^{3/2} e^{-(mv^2/2kT_e)} \tag{1.46}$$

Defining

$$u = \left( \frac{m}{2kT_e} \right)^{1/2} v \tag{1.47}$$

it can be shown that

$$v^3 \frac{\partial f^\circ}{\partial v} dv = -2n\pi^{-3/2} u^4 e^{-u^2} du \tag{1.48}$$

Substituting (1.49) into (1.45), we obtain

$$\begin{aligned}
 \sigma &= \frac{8ne^2}{3\sqrt{\pi}m} \left( \int_0^\infty \frac{\nu_m u^4 e^{-u^2}}{\omega^2 + \nu_m^2} du + i\omega \int_0^\infty \frac{u^4 e^{-u^2}}{\omega^2 + \nu_m^2} du \right) \\
 &= \sigma_R + i\sigma_I
 \end{aligned} \tag{1.49}$$

When the collision frequency  $\nu_m$  is independent of the electron speed  $v$ , then the real and imaginary parts of  $\sigma$  in (1.49) are given by

$$\sigma_R = \frac{\nu_m n e^2}{m(\omega^2 + \nu_m^2)} \tag{1.50}$$

$$\sigma_I = \frac{\omega n e^2}{m(\omega^2 + \nu_m^2)} \tag{1.51}$$

## 18 FUNDAMENTALS OF PLASMA CHEMISTRY

An expression for the free electron diffusivity can be derived by considering the problem of diffusion in the absence of an electric field. At steady state, (1.21) can then be written as

$$v \nabla_r f^\circ = -\nu_m \mathbf{f}' \quad (1.52)$$

Solving for  $\mathbf{f}'$  we obtain

$$\mathbf{f}' = -\frac{v}{\nu_m} \nabla_r f^\circ \quad (1.53)$$

Substituting (1.53) into the expression for the flux vector  $\Gamma$  given by (1.42) we obtain

$$\Gamma = -\frac{4\pi}{3} \int_0^\infty \frac{v^4}{m} \nabla_r f^\circ dv \quad (1.54)$$

The gradient of  $f^\circ$  appearing in (1.54) applies to the electron density portion of  $f^\circ$  alone, provided the electron speed is not a function of position. Under this restriction  $\nabla_r f^\circ$  may be written as

$$\nabla_r f^\circ = \frac{f^\circ}{n} \nabla_r n \quad (1.55)$$

Substituting (1.55) into (1.54) yields

$$\begin{aligned} \Gamma &= -\frac{4\pi}{3} \frac{1}{n} \nabla_r n \int_0^\infty \frac{v^4}{\nu_m} f^\circ dv \\ &= -D \nabla_r n \end{aligned} \quad (1.56)$$

where

$$D = \frac{4\pi}{3} \frac{1}{n} \int_0^\infty \frac{v^4}{\nu_m} f^\circ dv \quad (1.57)$$

is the free electron diffusivity.

If  $f^\circ$  is Maxwellian, (1.57) can be written as

$$D = \frac{8}{3\sqrt{\pi}} \frac{kT_e}{m} \int_0^\infty \frac{u^4}{\nu_m} e^{-u^2} du \quad (1.58)$$

When the momentum collision frequency can be assumed to be independent of electron speed, (1.58) reduces to

$$D = \frac{kT_e}{m\nu_m} \quad (1.59)$$

Under conditions where the distribution function is Maxwellian or can be approximated as Maxwellian, a useful relationship can be derived between the diffusion coefficient and the electron mobility  $\mu$ . For this purpose, we must define the mobility by

$$\begin{aligned}\mu &= \frac{\langle \mathbf{v} \rangle}{\mathbf{E}_e} \\ &= \frac{e}{m\nu_m}\end{aligned}\quad (1.60)$$

The ratio of  $D$  to  $\mu$ ,

$$\frac{D}{\mu} = \frac{kT_e}{e}\quad (1.61)$$

is known as the Einstein relation. When the distribution is non-Maxwellian, then the ratio  $D/\mu$  can be expressed as

$$\frac{D}{\mu} = \frac{m\langle v^2 \rangle}{3e}\quad (1.62)$$

when  $\nu_m$  is constant and

$$\frac{D}{\mu} = \frac{m}{2e} \frac{\langle v \rangle}{\langle 1/v \rangle}\quad (1.63)$$

when  $\sigma_m$  is constant.

The ratio  $D/\mu$  is a function of  $E_e/p$  and is known as the characteristic energy  $\varepsilon_k$ . Extensive measurements of  $\varepsilon_k$  for electron swarms have been reported for many gases [4,5,6]. As can be seen from (1.61) and (1.62),  $\varepsilon_k$  represents the average electron energy, provided that either  $f^\circ$  is Maxwellian or  $\nu_m$  is independent of electron speed. When neither of these conditions is satisfied, the characteristic energy is found to be a poor approximation of the average electron energy corresponding to a given value of  $E_e/p$ .

### Energy Transfer

The transfer of energy to a plasma occurs principally through the action of the electric field on the free electrons. The instantaneous rate of energy transfer per unit volume is given by

$$\bar{P}(t) = \sigma_r E_0 e^{i\omega t}\quad (1.64)$$

To obtain the net power dissipation, (1.64) is averaged over the period of one cycle of the field. For the case where  $\nu_m$  is independent of the electron velocity,

the time-averaged power density becomes

$$\bar{P} = \frac{ne^2E_0^2}{2m\nu_m} \left( \frac{\nu_m^2}{\nu_m^2 + \omega^2} \right) \quad (1.65)$$

or in terms of the effective field  $E_e$

$$\bar{P} = \frac{ne^2E_e^2}{m\nu_m} \quad (1.66)$$

From (1.65) we can observe that  $\nu_m$  must be finite for energy transfer to occur. Furthermore, the maximum value of  $\bar{P}$  is obtained when  $\omega^2 \ll \nu_m^2$  for a given value of  $E_0$ .

### Diffusion of Charged Species

We may turn next to a discussion of the spatial distribution of the charged particles in an ionized gas. At very low charge concentrations, such as those encountered near breakdown, electrons and positive ions will diffuse independently of each other and the flux of each species can be written as:

$$\Gamma_e = -D_e \nabla n_e \quad (1.67)$$

$$\Gamma_+ = -D_+ \nabla n_+ \quad (1.68)$$

where  $n_e$  and  $n_+$  denote the densities of electrons and positive ions, respectively. For steady-state conditions, the charged particles lost from the ionized gas by diffusion must be replaced by ionization. If the rate of ionization is represented by  $n_e\nu_i$ , where  $\nu_i$  is the ionization frequency, the steady-state conservation equations for electrons and positive ions will be given by

$$-\nabla \cdot \Gamma_e + n_e\nu_i = 0 \quad (1.69)$$

$$-\nabla \cdot \Gamma_+ + n_e\nu_i = 0 \quad (1.70)$$

Substitution of (1.67) and (1.68) into (1.69) and (1.70) gives

$$D_e \nabla^2 n_e + n_e\nu_i = 0 \quad (1.71)$$

$$D_+ \nabla^2 n_+ + n_e\nu_i = 0 \quad (1.72)$$

Equation (1.71) can be solved for a variety of plasma geometries in order to obtain the spatial distribution of electron density. We will consider two

examples here, that of a rectangular box and that of a cylindrical tube closed at its ends. For the rectangular geometry, (1.71) is expressed as

$$D_e \left( \frac{\partial^2 n_e}{\partial x^2} + \frac{\partial^2 n_e}{\partial y^2} + \frac{\partial^2 n_e}{\partial z^2} \right) + n_e v_i = 0 \quad (1.73)$$

The appropriate boundary conditions are given by:

$$\begin{aligned} \frac{\partial n_e}{\partial x} = 0 & \quad \text{at} \quad x = 0 & \quad \text{for all } y \text{ and } z \\ \frac{\partial n_e}{\partial y} = 0 & \quad \text{at} \quad y = 0 & \quad \text{for all } x \text{ and } z \\ \frac{\partial n_e}{\partial z} = 0 & \quad \text{at} \quad z = 0 & \quad \text{for all } x \text{ and } y \\ n_e = 0 & \quad \text{at} \quad x = \pm \frac{L}{2} & \quad \text{for all } y \text{ and } z \\ n_e = 0 & \quad \text{at} \quad y = \pm \frac{W}{2} & \quad \text{for all } x \text{ and } z \\ n_e = 0 & \quad \text{at} \quad z = \pm \frac{H}{2} & \quad \text{for all } x \text{ and } y \end{aligned} \quad (1.74)$$

where  $L$ ,  $W$ , and  $H$  represent the length, width, and height of the box. The solution to (1.73) and (1.74) is given by

$$n_e = n_{e0} \cos \left( \frac{\pi x}{L} \right) \cos \left( \frac{\pi y}{W} \right) \cos \left( \frac{\pi z}{H} \right) \quad (1.75)$$

where  $n_{e0}$  is the electron density at the center of the box. Substitution of this solution into the original differential equation leads to the constraint that

$$\frac{v_i}{D_e} = \frac{1}{\Lambda^2} = \left( \frac{\pi}{L} \right)^2 + \left( \frac{\pi}{W} \right)^2 + \left( \frac{\pi}{H} \right)^2 \quad (1.76)$$

where  $\Lambda$  is defined as the diffusion length.

## 22 FUNDAMENTALS OF PLASMA CHEMISTRY

For a cylindrical geometry, (1.71) takes the form

$$D_e \left[ \frac{1}{r} \frac{\partial}{\partial r} \left( r \frac{\partial n_e}{\partial r} \right) + \frac{\partial^2 n_e}{\partial z^2} \right] + n_e \nu_i = 0 \quad (1.77)$$

The boundary conditions in this case are

$$\begin{aligned} \frac{\partial n_e}{\partial r} &= 0 & \text{at } r &= 0 & \text{for all } z \\ \frac{\partial n_e}{\partial z} &= 0 & \text{at } z &= 0 & \text{for all } r \\ n_e &= 0 & \text{at } r &= R & \text{for all } z \\ n_e &= 0 & \text{at } z &= \pm \frac{L}{2} & \text{for all } r \end{aligned} \quad (1.78)$$

where  $R$  and  $L$  are the radius and length of the cylinder. The solution to (1.77) and (1.78) is given by

$$n_e = n_{e0} J_0 \left( \frac{2.405r}{R} \right) \cos \left( \frac{\pi z}{L} \right) \quad (1.79)$$

in which  $J_0$  represents the zeroth order Bessel function. Substitution of the solution for  $n_e$  back into (1.77) gives in this case

$$\frac{\nu_i}{D_e} = \frac{1}{\Lambda^2} = \left( \frac{2.405}{R} \right)^2 + \left( \frac{\pi}{L} \right)^2 \quad (1.80)$$

Solutions for the distribution of positive ions can now be obtained from (1.72), recognizing that  $\Gamma_e$  must equal  $\Gamma_+$  in order to maintain a zero flow of current at the boundaries of the ionized gas. From these considerations we obtain

$$n_+ = \frac{D_e}{D_+} n_e \quad (1.81)$$

Thus, at steady state the process of free diffusion leads to a concentration of positive ions considerably higher than that of electrons. Under these conditions, the ionized gas cannot be considered to be a plasma.

The separation of charge caused by the difference in diffusion coefficients of electrons and ions produces a space charge field. The magnitude of this

field will remain small, however, as long as the charge concentrations remain low ( $n_e < 10^2 \text{ cm}^{-3}$ ) and as a result will not affect the diffusion of either charge carrier.

As the charge concentration is increased, a level is finally reached where  $\lambda_D \ll \Lambda$  and the medium may properly be termed a plasma. Under these conditions the space charge field  $\mathbf{E}_{sc}$  becomes sufficiently large to affect the transport of both electrons and positive ions. The expressions for charge flux are now given by

$$\mathbf{\Gamma}_e = -D_e \nabla n_e - n_e \mu_e \mathbf{E}_{sc} \quad (1.82)$$

$$\mathbf{\Gamma}_+ = -D_+ \nabla n_+ + n_+ \mu_+ \mathbf{E}_{sc} \quad (1.83)$$

Equations (1.82) and (1.83) can be used to solve for  $\mathbf{E}_{sc}$  if we assume  $n_e = n_+ = n$  and take  $\mathbf{\Gamma}_e = \mathbf{\Gamma}_+ = \mathbf{\Gamma}$  as before. These are the conditions required for ambipolar diffusion and lead to an expression for  $\mathbf{E}_{sc}$  as

$$\mathbf{E}_{sc} = - \frac{(D_e - D_+) \nabla n}{(\mu_e + \mu_+) n} \quad (1.84)$$

Substitution of (1.84) into either (1.82) or (1.83) gives

$$\mathbf{\Gamma} = - \left( \frac{D_+ \mu_e + D_e \mu_+}{\mu_e + \mu_+} \right) \nabla n = -D_a \nabla n \quad (1.85)$$

in which  $D_a$  is defined as the ambipolar diffusivity. Since  $\mu_e \gg \mu_+$  the magnitude of  $D_a$  can be approximated by

$$D_a \simeq D_+ \left( 1 + \frac{D_e \mu_+}{D_+ \mu_e} \right) = D_+ \left( 1 + \frac{T_e}{T_g} \right) \quad (1.86)$$

Ambipolar diffusion will usually occur when  $n_e \simeq n_+ \simeq 10^8 \text{ cm}^{-3}$  and the distribution of both charged species will then be governed by

$$D_a \nabla^2 n + n \nu_1 = 0 \quad (1.87)$$

Equation (1.87) has the identical form of (1.71). As a result, the solutions for  $n_e$  and  $n_+$  will have the same form as (1.75) and (1.79) with the exception that  $D_a$  will replace  $D_e$  in the expressions for  $\Lambda$ .

In the transition region between free and ambipolar diffusion, the space charge field cannot be represented by (1.84). To solve for the charge distribution it now becomes necessary to consider Poisson's equation in addition

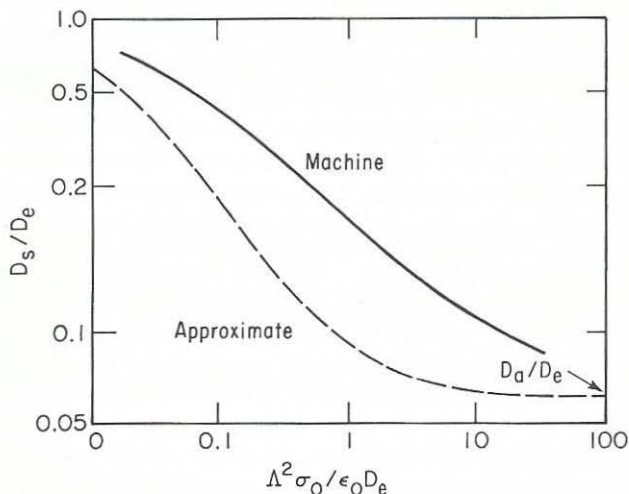


FIGURE 1.7. The effective diffusivity as a function of the plasma conductivity [7].

to the conservation equation for each species. Allis and Rose [7] have solved this set of three equations for the system of a discharge sustained between two infinite parallel planes. In the course of their analysis an effective diffusivity was defined as

$$D_s = D_a \left( 1 + \frac{\mu_e \rho}{\sigma} \right) \quad (1.88)$$

where

$$\rho = (n_+ - n_e)e \quad (1.89)$$

and

$$\sigma = (\mu_+ n_+ + \mu_e n_e)e \quad (1.90)$$

Figure 1.7 illustrates the value of  $D_s$  at the center of the discharge as a function of the central conductivity  $\sigma_0$ . Also shown in this figure is an approximation for  $D_s$  derived from the expression

$$D_s = D_a \frac{D_e + \Lambda^2 \sigma_0 / \epsilon_0}{D_a + \Lambda^2 \sigma_0 / \epsilon_0} \quad (1.91)$$

From Figure 1.7 and (1.91), we see that  $D_s = D_e$  when  $\sigma_0 \approx 0$ , and that  $D_s$  decreases as the central conductivity increases. For large values of  $\sigma_0$ ,  $D_s$  approaches the ambipolar value  $D_a$ .

When a significant concentration of negative ions is present in addition to the positive ions, the diffusion of electrons must be considered as part of

a three-particle system. The appropriate flux equations are now

$$\Gamma_e = -D_e \nabla n_e - \mu_e n_e \mathbf{E}_{sc} \quad (1.92)$$

$$\Gamma_- = -D_- \nabla n_- - \mu_- n_- \mathbf{E}_{sc} \quad (1.93)$$

$$\Gamma_+ = -D_+ \nabla n_+ + \mu_+ n_+ \mathbf{E}_{sc} \quad (1.94)$$

An expression for the space charge field can be obtained by substituting (1.92)–(1.94) into the equation for a current balance

$$\Gamma_+ = \Gamma_e + \Gamma_- \quad (1.95)$$

Thus

$$\mathbf{E}_{sc} = \frac{-D_e \nabla n_e - D_- \nabla n_- + D_+ \nabla n_+}{\mu_e n_e + \mu_- n_- + \mu_+ n_+} \quad (1.96)$$

Substitution of (1.96) together with the charge neutrality condition  $n_+ = n_e + n_-$  into (1.92) gives

$$\Gamma_e = - \left\{ \frac{[D_e(\mu_- + \mu_+)n_- + (D_e\mu_+ + D_+\mu_e)]\nabla n_e + \mu_e n_e(D_+ - D_-)\nabla n_-}{(\mu_e + \mu_+)n_e + (\mu_- + \mu_+)n_-} \right\} \quad (1.97)$$

Since  $D_+ \simeq D_-$ , the term in the numerator of (1.97) containing the difference between the two diffusion coefficients can be neglected. If the dimensionless groups

$$\beta = \frac{n_-}{n_e} \quad (1.98)$$

$$\phi = \frac{D_e \mu_+}{\mu_e D_+} = \frac{D_e \mu_-}{\mu_e D_-} = \frac{T_e}{T_{\pm}}$$

are introduced, (1.97) can finally be written as

$$\Gamma_e = -D_+ \left[ \frac{1 + \phi + 2\beta\phi}{1 + (1 + \beta)\mu_+/\mu_e + \beta\mu_+/\mu_e} \right] \nabla n_e$$

$$= -D_{a_e} \nabla n_e \quad (1.99)$$

Figure 1.8 shows the behavior of  $D_{a_e}/D_+$  as a function of  $\beta$  and  $\phi$ . As  $\beta$  increases,  $D_{a_e}$  increases until it reaches a maximum value of  $D_{a_e} = D_e$ . At

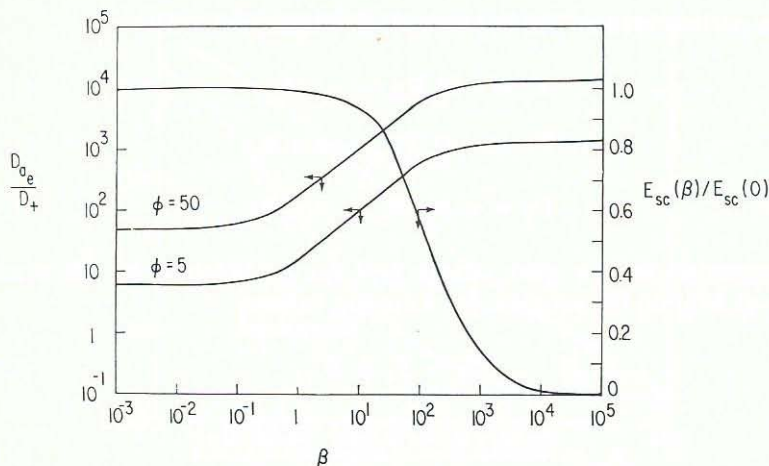


FIGURE 1.8. Variation of the ambipolar diffusivity and the space charge field in an oxygen plasma as a function of the relative concentration of negative ions.

this point the electrons are in free diffusion. The cause for the increase of  $D_{a_e}$  with  $\beta$  is the reduction in the space charge field as illustrated by Figure 1.8.

#### 1.4. CHEMICAL REACTIONS OCCURRING IN PLASMAS

A broad spectrum of reactions have been observed to take place in plasmas. These include reactions between electrons and molecules, ions and molecules, ions and ions, and electrons and ions. Due to the very large number of such processes occurring when only one parent gas is present, we shall not attempt to provide a comprehensive discussion of this subject here. Instead, we shall illustrate the diversity of plasma reactions by examining in detail the processes occurring in an oxygen discharge. The reader who is interested in pursuing this subject as it applies to other gases should consult the books by McDaniel [5], McDaniel et al. [8], and Massey, Burhop, and Gilbody [6].

We may begin our discussion of electron-molecule reactions involving oxygen by considering the potential energy diagram for  $O_2$  shown in Figure 1.9. The ground state is designated by the spectroscopic symbol  $X^3\Sigma_g^-$ . Above this lie four higher states,  $a^1\Delta_g$ ,  $b^1\Sigma_g^+$ ,  $C^3\Delta_u$ , and  $A^3\Sigma_u^+$ , all of which dissociate into ground-state atoms. Oxygen in the metastable  $a^1\Delta_g$  state is known as "singlet" oxygen. This species is particularly long-lived and participates in

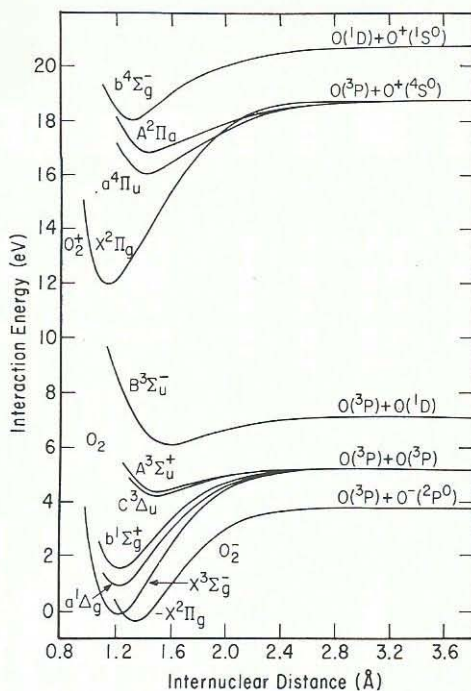


FIGURE 1.9. Potential energy curves for some states of  $O_2^-$ ,  $O_2$ , and  $O_2^+$ .

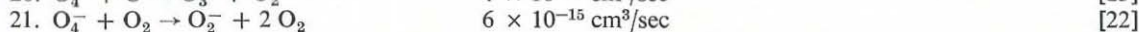
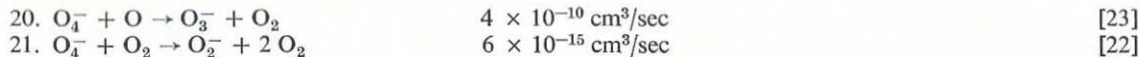
a number of chemical reactions in oxygen discharges (see Table 1.1). The next highest state is the  $B^3\Sigma_u^-$ . Vertical excitation to this state from the ground state leads to dissociation producing one ground-state atom and one singlet D atom. Further excitation leads to the ionization of the molecule and the formation of  $O_2^+$  in the  $X^2\Pi_g$  state.

Electrons colliding with molecules of oxygen undergo either elastic or inelastic collisions. In the former, the molecule is left in an unexcited state but gains  $2m/M$  of the original kinetic energy of the electron. This process leads to a slight increase in the kinetic energy of the molecule and, when repeated frequently, is responsible for the increase in the gas temperature. The probability of elastic collisions is characterized by the momentum cross-section  $\sigma_m$ . Figure 1.10 illustrates the magnitude of  $\sigma_m$  for oxygen as a function of electron energy.

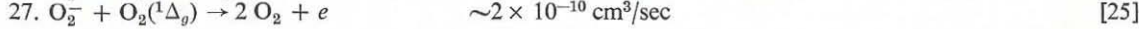
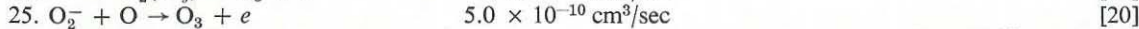
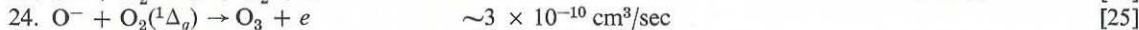
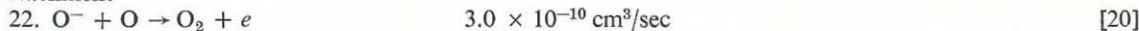
At low electron energies, the principal inelastic processes which occur are the excitation of rotational and vibrational levels of ground-state  $O_2$ . Very little experimental data has been obtained related to the cross-sections for rotational excitation and the best estimates of their size are the theoretical

**TABLE 1.1.** Elementary Reactions Occurring in an Oxygen Discharge

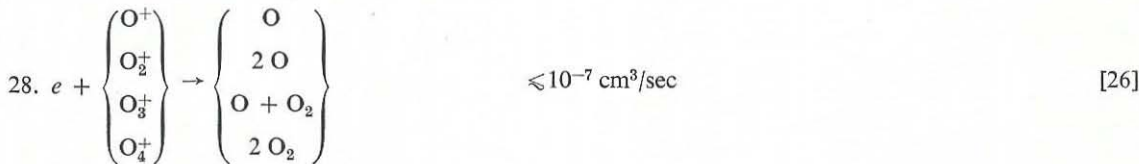
Reaction	$k$	$\sigma_{\max}$ (cm <sup>2</sup> )	Reference
<b>Ionization</b>			
1. $e + O_2 \rightarrow O_2^+ + 2e$		$2.72 \times 10^{-16}$	[9]
2. $e + O \rightarrow O^+ + 2e$		$1.54 \times 10^{-18}$	[10]
<b>Dissociative ionization</b>			
3. $e + O_2 \rightarrow O^+ + O$		$1.0 \times 10^{-16}$	[11]
<b>Dissociative attachment</b>			
4. $e + O_2 \rightarrow O^- + O$		$1.41 \times 10^{-18}$	[12]
5. $e + O_2 \rightarrow O^- + O^+ + e$		$4.85 \times 10^{-19}$	[12]
<b>Dissociation</b>			
6. $e + O_2 \rightarrow 2O + e$		$2.25 \times 10^{-18}$	[13]
<b>Metastable formation</b>			
7. $e + O_2 \rightarrow O_2(^1\Delta_g) + e$		$3.0 \times 10^{-20}$	[13]
<b>Charge transfer</b>			
8. $O^+ + O_2 \rightarrow O_2^+ + O$	$2 \times 10^{-11}$ cm <sup>3</sup> /sec		[14]
9. $O_2^+ + O \rightarrow O^+ + O_2$		$8 \times 10^{-16}$	[15]
10. $O_2^+ + O_2 \rightarrow O_3^+ + O$		$1 \times 10^{-16}$	[16]
11. $O_2^+ + 2O_2 \rightarrow O_4^+ + O_2$	$2.8 \times 10^{-30}$ cm <sup>6</sup> /sec $2.5 \times 10^{-14}$ cm <sup>3</sup> /sec at $E/p = 20$ V/cm torr		[17]
12. $O^- + O_2 \rightarrow O_2^- + O$	$3.4 \times 10^{-12}$ cm <sup>3</sup> /sec at $E/p = 45$ V/cm torr		[18]
13. $O^- + O_3 \rightarrow O_3^- + O$	$5.3 \times 10^{-10}$ cm <sup>3</sup> /sec		[19]
14. $O^- + 2O_2 \rightarrow O_3^- + O_2$	$1.0 \pm 0.2 \times 10^{-30}$ cm <sup>6</sup> /sec		[18]
15. $O_2^- + O \rightarrow O^- + O_2$	$5 \times 10^{-10}$ cm <sup>3</sup> /sec		[20]
16. $O_2^- + O_2 \rightarrow O_3^- + O$		$< 10^{-18}$	[21]
17. $O_2^- + O_3 \rightarrow O_3^- + O_2$	$4.0 \times 10^{-10}$ cm <sup>3</sup> /sec		[19]
18. $O_2^- + 2O_2 \rightarrow O_4^- + O_2$	$3 \times 10^{-31}$ cm <sup>6</sup> /sec		[22]
19. $O_3^- + O_2 \rightarrow O_2^- + O_3$		$4 \times 10^{-17}$	[21]



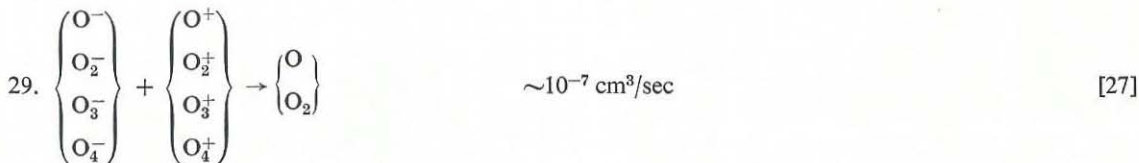
#### Detachment



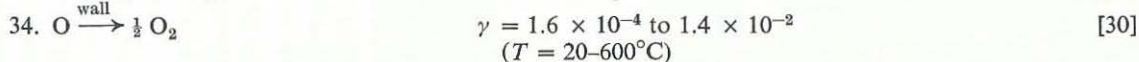
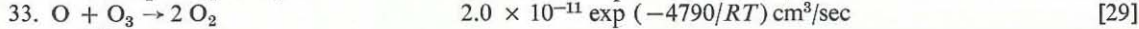
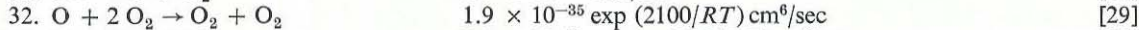
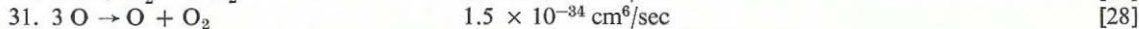
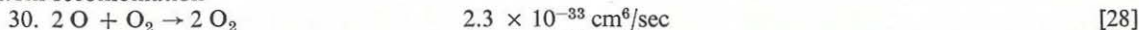
#### Electron-ion recombination



#### Ion-ion recombination



#### Atom recombination



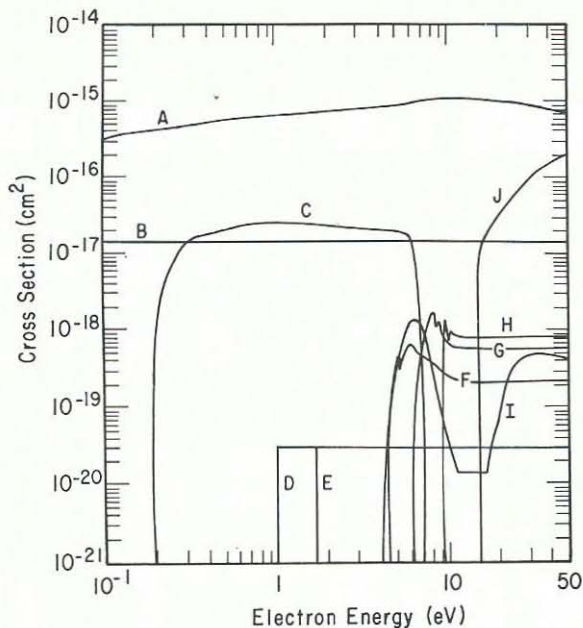


**FIGURE 1.10.** Elastic and inelastic collision cross-sections for electrons in oxygen; (A) elastic scattering; (B) rotational excitation; (C) vibrational excitation; (D) excitation to the  $a^1\Delta_g$  state; (E) excitation of the  $b^1\Sigma_u^+$  state; (F) excitation of the  $A^3\Sigma_u^+$  state; (G) excitation of the  $B^3\Sigma_u^-$  state; (H) excitation of higher electronic states; (I) dissociative attachment; (J) ionization [13].

calculations presented by Gerjuoy and Stein [31]. A curve representing the sum of all rotational excitations is shown in Figure 1.10. Cross-sections for the excitation of individual vibrational levels, calculated by Hake and Phelps [32], are shown in Figure 1.11. The total cross-section for vibrational excitation is shown in Figure 1.10.

For electron energies above 1 eV it becomes possible to excite higher electronic levels. The cross-sections for some of these processes are illustrated in Figure 1.10. In each case the magnitude of the cross-section rises very rapidly near the threshold energy and attains a maximum value at several electron volts above the threshold.

Because of its electronegative nature, oxygen is able to form negative ions either by direct attachment or by dissociative attachment. The former process requires a three-body collision involving an electron and two oxygen molecules. Attachment by this means produces an  $O_2^-$  ion and the second molecule carries away the attachment energy. A curve for the potential energy

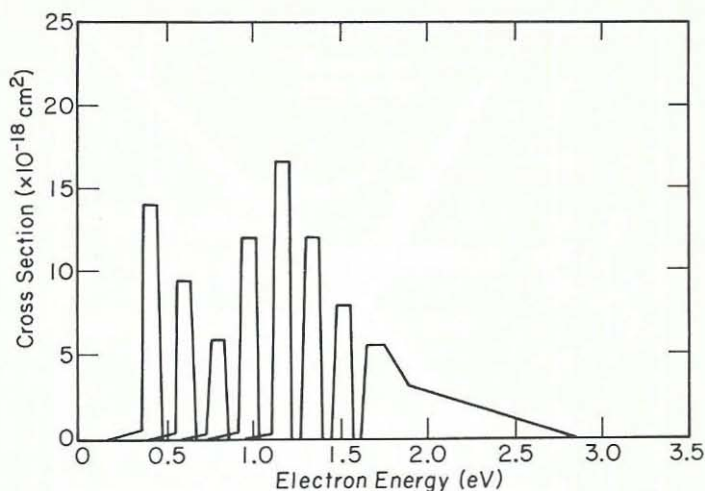
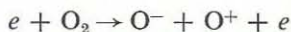


FIGURE 1.11. Vibrational excitation cross-sections for electrons in oxygen [32].

of  $O_2^-$  is illustrated in Figure 1.9. By contrast, dissociative attachment is a two-body process leading to the formation of an  $O^-$  ion and an oxygen atom. The cross-section for this process is shown in Figure 1.10. It should be noted that the cross-section exhibits two maxima, the first corresponding to the process



and the second to the process



Reaction rate constants for the processes described above can be derived from the following relationship

$$k_i = \int_0^{\infty} \left( \frac{\gamma \varepsilon}{2m} \right)^{1/2} \sigma_i(\varepsilon) f(\varepsilon) d\varepsilon \quad (1.100)$$

where  $\varepsilon$  is the electron energy,  $\sigma_i$  the cross-section for the  $i$ th process, and  $f(\varepsilon)$  the electron-energy distribution function. For a rigorous calculation of the rate constant  $k_i$ , the exact form of the electron-energy distribution function should be used. Since the determination of this function is difficult (see Section 1.2), it is desirable to determine to what degree a Maxwellian distribution might be used as an approximation.

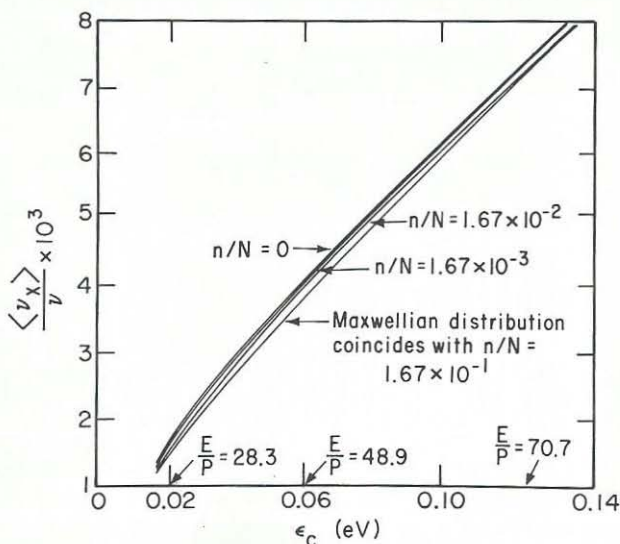
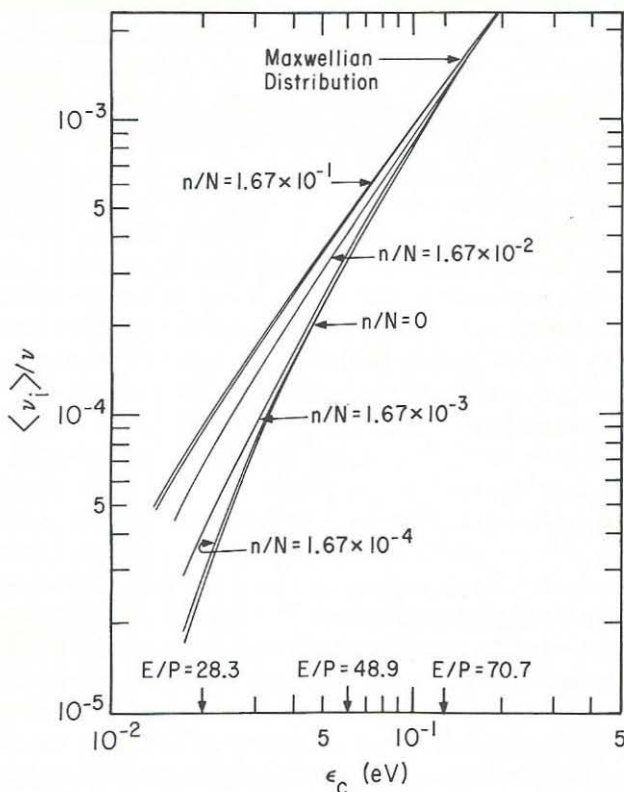


FIGURE 1.12. The ratio of the average inelastic collision frequency to the elastic collision frequency as a function of the energy parameter  $\epsilon_c$  and the extent of ionization in a hydrogen plasma [2].

Dreicer [2] has discussed this problem for the case of a hydrogen plasma. In this work, solutions to the Boltzmann equation were obtained which took into account the effects of coulombic interactions between electrons and as well as elastic and inelastic interactions between electrons and molecular hydrogen. The electron-energy distribution functions (see Figs. 1.3–1.5) derived by this means were then used to determine the ratio of the average inelastic collision rate to the elastic collision rate as a function of the average energy transferred upon collision. These results are shown in Figure 1.12 for different values of the degree of ionization. Values of  $\langle \nu_x \rangle / \nu$  computed for a Maxwellian distribution function are also shown in this figure. As can be seen, the values of  $\langle \nu_x \rangle / \nu$  show very little dependence on either the degree of ionization or the form of the distribution function. The principal cause of these observations is that the true electron-energy distribution differs very little from a Maxwellian form over the range of energies of interest in evaluating  $\langle \nu_x \rangle$ .

By contrast, Dreicer's computations of the ratio of the average ionization rate to the elastic collision rate show a strong influence of both the degree of ionization and the form of the distribution function. These results are shown in Figure 1.13. In this instance differences in the values of  $\langle \nu_i \rangle$  are the result of differences in the tail of the distribution function (see Fig. 1.4).



**FIGURE 1.13.** The ratio of the average ionization frequency to the elastic collision frequency as a function of the energy parameter  $\epsilon_c$  and the extent of ionization in a hydrogen plasma [2].

On the basis of Dreicer's work we may conclude that the use of a Maxwellian distribution function to calculate rate constants is justified provided the threshold for the process being considered is not much larger than the average electron energy. Further substantiation of this conclusion can be derived from the work of Myers [33]. In this case, the distribution function was evaluated for an electron swarm in oxygen. Computations of the average dissociative attachment cross-section as a function of the average electron energy showed that very nearly the same values were obtained using the true distribution function and a Maxwellian distribution function.

The elastic and inelastic collisions which electrons undergo in the plasma lead to a loss of energy from the electron cloud. These energy losses are compensated by the gain of energy from the electric field. When the plasma

reaches a steady state, the rate of energy gain from the field just balances the loss of energy due to electron-molecule collisions as well as other loss processes. An expression for the energy balance is given by

$$\bar{P} = \frac{2m}{M} \langle \varepsilon \rangle k_m n N + \sum_j \varepsilon_j k_j n N + \langle \varepsilon \rangle k_i n N + \langle \varepsilon \rangle k_d n \quad (1.101)$$

where  $\langle \varepsilon \rangle$  is the average electron energy,  $\varepsilon_j$  is the energy loss for the  $j$ th process,  $k_m = \nu_m/N$  is the rate constant for momentum transfer,  $k_j$  is the rate constant for the  $j$ th inelastic process,  $k_i$  is the ionization rate constant, and  $k_d = D_a/\Lambda^2$  is the effective diffusion rate constant. The first two terms in (1.101) account for the loss of energy by elastic and inelastic collisions, respectively. The third term accounts for the energy needed to bring each newly formed electron up to the average electron energy. The fourth term describes the loss of energy associated with ambipolar diffusion. The fraction of the total power which is dissipated in any one process can be evaluated by dividing the rate of energy loss for that process by the total power. As can be seen from (1.101), the fractional loss of energy is independent of  $n$  and only depends upon the magnitudes of  $k_m$ ,  $k_j$ , and  $k_d$ . Since the rate constants for the collisional processes are functions of  $E_e/p$ , the fractional loss of energy may also be expressed in terms of this parameter.

Figure 1.14 illustrates the fractional energy losses for a variety of processes occurring in oxygen. At low values of  $E_e/p$ , the principal loss of energy occurs through the excitation of vibrational states. As  $E_e/p$  is increased, ever larger fractions of the total power are consumed by various electronic excitation processes. With the exception of ionization, the losses for these processes exhibit a maximum. This characteristic is due in part to the shape of the collision cross-sections (see Fig. 1.10) and in part to the very rapid increase in the losses associated with ionization. In contrast to the inelastic processes, the loss of energy through elastic collisions remains small throughout the range of  $E_e/p$ , which means that not more than about 1.5% of the total power is directed towards heating the gas.

The positive and negative ions produced by electron collisions with the molecules of the sustaining gas can react further to produce a large number of new ionic species. As an example, we may look at the reactions which occur in an oxygen discharge. The elementary steps involved in the formation and loss of all of the observed species are listed in Table 1.1. Most of the ionic reactions appearing in Table 1.1 are exothermic and hence proceed at a rate which is essentially independent of ion energy. Processes such as the charge transfer reactions 9, 10, 16, and 19, and the collisional detachment reactions 23 and 26 are endothermic and proceed only if the ion energy is sufficient to surpass the activation energy for the reaction. To determine the effective ion temperature as a function of the applied field, it is recommended

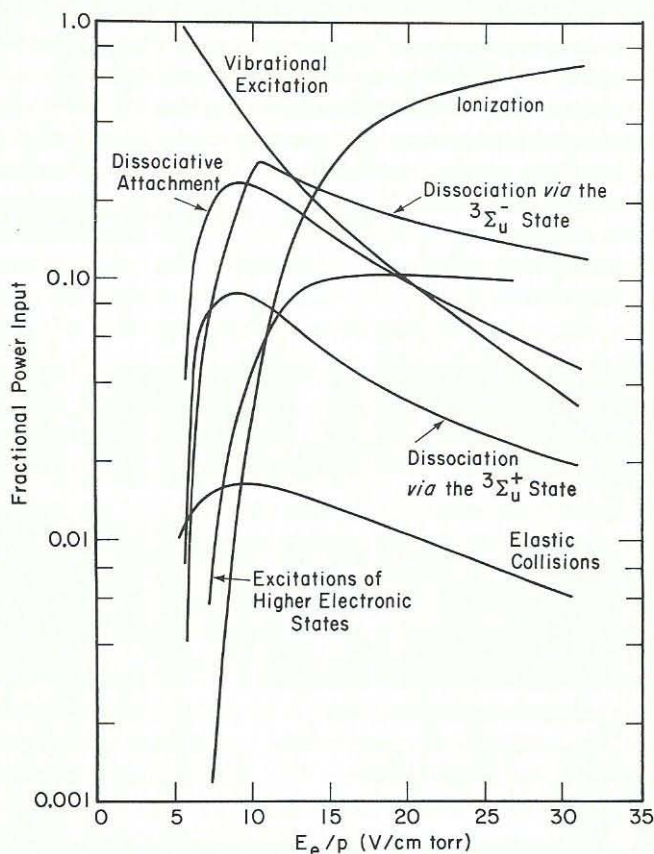


FIGURE 1.14. The fractional power input to elastic and inelastic collisions as a function of  $E_e/p$  for oxygen [34].

that Wannier's relationship

$$\frac{3}{2}kT_i = \frac{1}{2}(M_i + M)v_d^2 + \frac{3}{2}kT_g \quad (1.102)$$

be used. In (1.102)  $T_i$  is the ion temperature,  $M_i$  the mass of the ion,  $M$  the mass of the neutral gas molecule, and  $v_d$  the drift velocity of the ion, which is a function of  $E_e/p$ .

## 1.5 PHYSICAL CHARACTERISTICS OF HIGH-FREQUENCY DISCHARGES

### Breakdown and Steady-State Operating Conditions

As was discussed in the previous sections, the value of  $E_e/p$  in a plasma plays an important role in determining the properties of the plasma and the rates

at which chemical processes occurring in it proceed. Consequently, we wish to develop methods for predicting  $E_e/p$  both at breakdown and under steady-state operating conditions. Since the rates of all processes involving electron-molecule collisions are proportional to the electron density, it will be necessary to determine this quantity as well. To begin our discussion we shall consider the evaluations of  $E_e/p$  and  $n$  for a plasma in which the field strength is constant throughout the plasma.

[The breakdown of a gas in an electric field will occur when the rate of ionization becomes sufficiently large to balance the loss of electrons by various processes]. If the principal loss mechanism is considered to be free electron diffusion, then breakdown will be achieved when the condition

$$v_i = \frac{D_e}{\Lambda^2} \quad (1.103)$$

is satisfied.

Equation (1.103) can be used to determine the magnitude of the breakdown field. For this purpose it is first rewritten as

$$\frac{v_i}{p} = \frac{D_{e1}}{(p\Lambda)^2} \quad (1.104)$$

where  $D_{e1}$  is the free electron diffusivity evaluated at 1 torr. The quantity  $v_i/p$  essentially represents the ionization constant  $k_i = v_i(RT/p)$  and is thus a function of  $E_e/p$  [see (1.100) in Section 1.4]. As a result, we see that for a fixed value of  $p\Lambda$  (1.104) will be satisfied by only one value of  $E_e/p$ . An illustration of the relationships between  $p\Lambda$ ,  $v_i/p$  and  $E_e/p$  is shown in Figure 1.15.

Figure 1.16 shows a curve of  $E_e/p$  versus  $p\Lambda$  for the breakdown of hydrogen between two parallel plate electrodes. Notice that, at low values of  $p\Lambda$ ,  $E_e/p$  is quite large due to the rapid loss of electrons under these conditions. As  $p\Lambda$  increases,  $E_e/p$  decreases and tends to level out. These characteristics are due to the reduced loss of electrons by diffusion and the shape of the plot of  $v_i/p$  versus  $E_e/p$ . It should be noted that the actual value of the applied field will vary with frequency since  $E_e$  is defined as  $E_0[v_m^2/2(v_m^2 + \omega^2)]^{1/2}$ . Thus when  $\omega^2 \ll v_m^2$ ,  $E_e = E_0/\sqrt{2}$  and when  $\omega^2 \gg v_m^2$ ,  $E_e \simeq E_0 v_m/\sqrt{2}\omega$ .

Under certain conditions, mechanisms other than electron diffusion may control the breakdown-field strength. Thus, we must define the limits within which diffusion-controlled breakdown is valid. In Figure 1.17 these limits are illustrated on a plot of  $p\Lambda$  versus  $p\lambda$  where  $\lambda$  is the wave length of the applied field. The uniform field line defines the limit at which the field can no longer be considered uniform across the gap separating the electrodes. The mean free-path line describes the limit at which the electron mean free path becomes

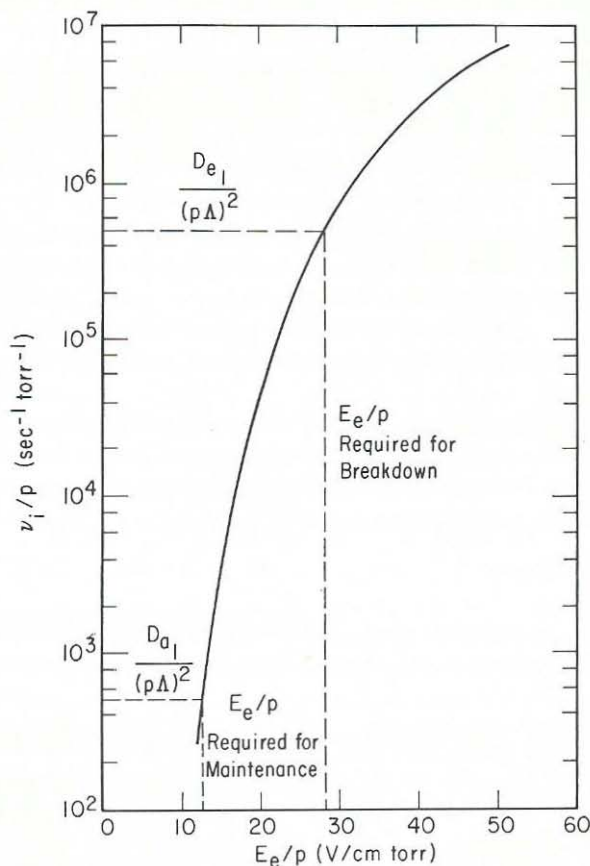


**FIGURE 1.15.** Illustration of the breakdown and maintenance values of  $E_e/p$  on a plot of the reduced ionization frequency versus  $E_e/p$  for hydrogen.

comparable to the interelectrode gap. Finally, the oscillation amplitude line describes the limit at which the excursion of an electron during one quarter of a cycle becomes comparable to one half of the interelectrode gap. Within the region defined by the three limiting lines, breakdown is controlled by diffusion.

When breakdown occurs in an electronegative gas, electrons can be lost through attachment to form negative ions in addition to being lost by diffusion. Under such conditions (1.104) must be defined as

$$\frac{\nu_i - \nu_a}{p} = \frac{D_{e1}}{(p\Delta)^2} \quad (1.105)$$

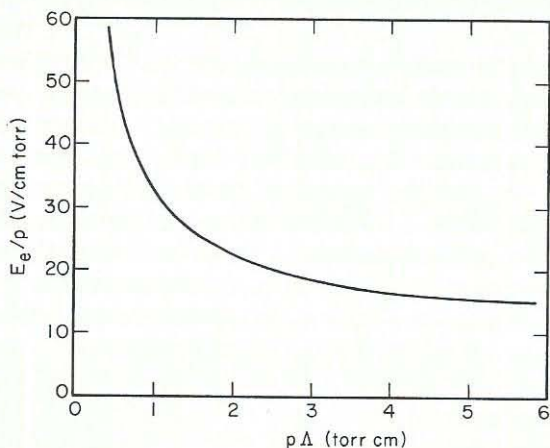


FIGURE 1.16. The value of  $E_e/p$  as a function of  $p\Delta$  required for breakdown in hydrogen.

where  $\nu_a$  is the electron attachment frequency. The breakdown-field strength can then be determined as explained above, provided information is available on  $\nu_i/p$  and  $\nu_a/p$  as functions of  $E_e/p$ .

As the electron density is increased from zero near breakdown to higher values, the effective electron diffusivity decreases until it reaches the ambipolar value. This pattern was shown in Figure 1.7. Due to the decrease in

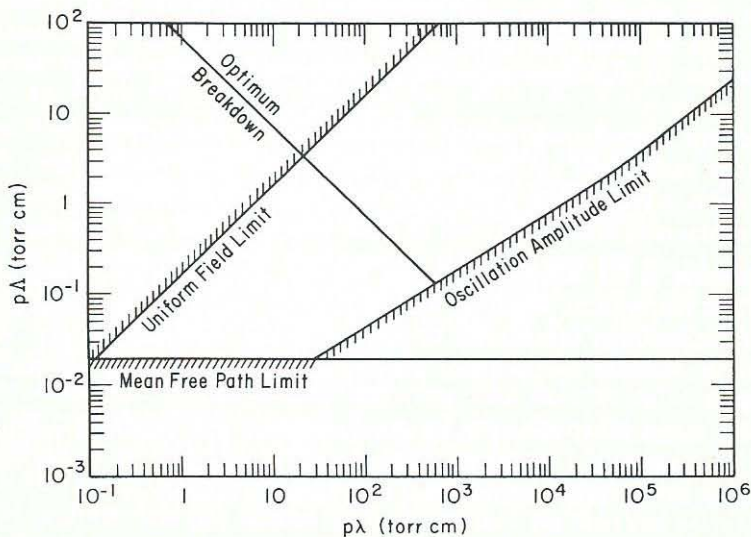


FIGURE 1.17. A plot of the limits of the diffusion theory for high-frequency breakdown [35].

the diffusion coefficient, the value of  $\nu_i/p$  needed to sustain a steady-state discharge will be reduced and will approach a lower limit given by

$$\frac{\nu_i}{p} = \frac{D_{a1}}{(p\Lambda)^2} \quad (1.106)$$

when  $n_e$  exceeds  $10^8 \text{ cm}^{-3}$ . The decrease in  $\nu_i/p$  in turn causes a decrease in the value of  $E_e/p$  as is shown in Figure 1.15 and represents the final consequence of the increase in electron density.

Rose and Brown [36] have demonstrated that the effects of  $p\Lambda$  and  $n$  on the steady-state value of  $E_e/p$  can be summarized on a single plot. Figure 1.18 illustrates their results for a hydrogen discharge maintained between two parallel plate electrodes. The electron density at the midplane is given by  $n_0$ . As we can see, for a fixed value of  $p\Lambda$ ,  $E_e/p$  decreases from its value at breakdown, corresponding to the point on the curve marked  $n_0\Lambda^2 = 0$ , to a lower limit achieved when the electron density is very large. This limiting value of  $E_e/p$  occurs when  $D_s = D_a$ . The effects of a change in  $p\Lambda$  are also readily observed in Figure 1.18. As the value of  $p\Lambda$  is increased,  $E_e/p$  is decreased for a given value of  $n_{e0}$ . However, when  $n_0\Lambda^2 \approx 10^9 \text{ cm}^{-3}$ ,  $E_e/p$  becomes independent of the electron density and is then a function of  $p\Lambda$  alone.

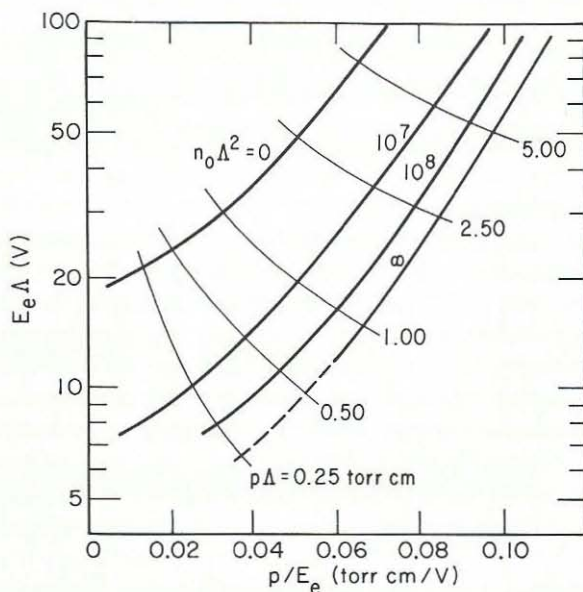


FIGURE 1.18. Theoretical calculations of  $E_e/p$  as a function of  $p\Lambda$  and  $n_0\Lambda^2$  for hydrogen [36].

The electron density in the high-frequency glow discharges used in most plasma-chemistry studies lie in the range of  $10^{10}$ – $10^{12}$   $\text{cm}^{-3}$ . These levels are sufficiently high to make  $E_e/p$  independent of the electron density as shown in Figure 1.18.

When the value of  $E_e/p$  becomes independent of the electron density, the electron density can be evaluated directly from the expression for the power density

$$\bar{P} = \frac{ne^2E_e^2}{m\nu_m} \quad (1.107)$$

Equation (1.107) can be rewritten in the following form

$$\frac{n}{\bar{P}\Lambda} = \frac{m\nu_{m1}}{[e^2p\Lambda(E_e/p)^2]} \quad (1.108)$$

where  $\nu_{m1}$  is the value of  $\nu_m$  at 1 torr. Since the right-hand side of (1.108) is a function of  $p\Lambda$  alone,  $n/\bar{P}\Lambda$  can be plotted as a function of  $p\Lambda$ . Figure 1.19 shows a plot of both  $E_e/p$  and  $n/\bar{P}\Lambda$  versus  $p\Lambda$  for a discharge in oxygen.

From Figure 1.19 we can conclude that, given the discharge dimensions and hence  $\Lambda$ , the gas pressure  $p$ , and the power density  $\bar{P}$ , we can determine  $E_e/p$  and  $n$ . Since  $E_e/p$  defines the electron-energy distribution function, a complete description of the physical properties of the discharge is now possible.

### Electric Field and Electron-Density Distributions

The discussion of maintenance fields up to this point has considered the field to be uniform throughout the plasma. This condition is satisfied for electric fields applied in a direction perpendicular to the gradient in electron density or for very high-frequency fields regardless of their orientation. Thus, it is appropriate to discuss the distribution of electric-field strength for intermediate driving frequencies and situations where the field is parallel to the gradient in electron density.

Let us consider a discharge sustained between two infinite parallel plate electrodes placed on the outside of a dielectric container, as shown in Figure 1.20. For this geometry, the width of the discharge zone is the only important linear dimension.

The analysis of the spatial distribution of the electric field can be initiated by recognizing that the sum of conduction and displacement currents must remain constant for the geometry considered. This may be expressed as

$$J = \sigma E + \epsilon_0 \frac{\partial E}{\partial t} \quad (1.109)$$

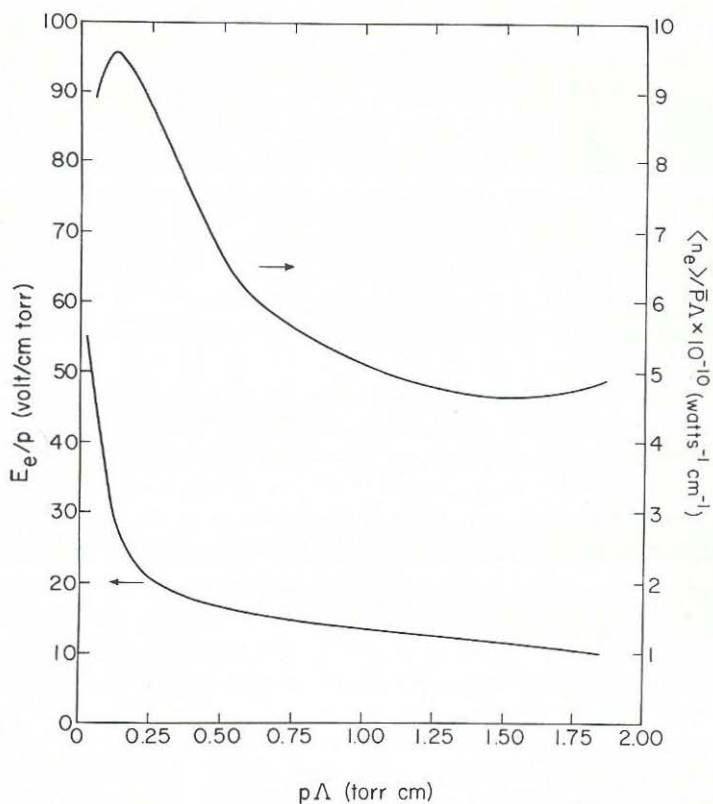


FIGURE 1.19. The values of  $E_e/p$  and  $n_e/\bar{P}\Delta$  as a function of  $p\Delta$  for a steady-state discharge in oxygen.

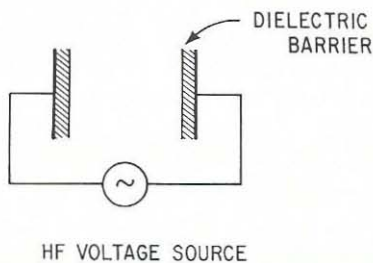


FIGURE 1.20. Schematic of a high-frequency discharge.

in which  $J$  is taken to be constant. For a purely sinusoidal electric field,  $E = |E| e^{i\omega t}$  and the conductivity  $\sigma$  can be expressed as

$$\sigma = \frac{ne^2(\nu_m - i\omega)}{m(\nu_m^2 + \omega^2)} \quad (1.110)$$

Substituting the expressions for the electric field and the conductivity into (1.109), we obtain

$$J = \left\{ \frac{ne^2}{m} \left( \frac{\nu_m}{\nu_m^2 + \omega^2} \right) + i\omega\epsilon_0 \left[ 1 - \frac{ne^2}{m\epsilon_0} \left( \frac{1}{\nu_m^2 + \omega^2} \right) \right] \right\} E \quad (1.111)$$

Equation (1.105) can be put in a more convenient form by rewriting it in terms of  $r = ne^2/m\epsilon_0\omega^2$ , a dimensionless electron density, and  $\alpha = \nu_m/\omega$ , a dimensionless collision frequency. Thus,

$$J = \left\{ \epsilon_0\omega r \left( \frac{\alpha}{1 + \alpha^2} \right) + i\epsilon_0\omega \left[ 1 - r \left( \frac{1}{1 + \alpha^2} \right) \right] \right\} E \quad (1.112)$$

Taking the magnitude of (1.112), we arrive at the desired expression

$$|E| = \frac{|J|}{\epsilon_0\omega} \left[ \frac{(1 + \alpha^2)}{(r - 1)^2 + \alpha^2} \right]^{1/2} \quad (1.113)$$

Equation (1.113) allows us to calculate the magnitude of the field at any position, provided the total current density and the local electron density are known. For conditions in which  $r \ll 1$ , (1.113) reduces to  $|E| = |J|/\epsilon_0\omega$  which represents the field across a parallel plate capacitor. At lower frequencies or higher electron densities,  $r \gtrsim 1$ . In these cases (1.113) can be conveniently rewritten as

$$E = E_0 \left[ \frac{(r_0 - 1)^2 + \alpha^2}{(r - 1)^2 + \alpha^2} \right]^{1/2} \quad (1.114)$$

where the subscript zero denotes conditions at the center of the discharge. It should be noted that from this point on,  $E$  refers to the magnitude of the electric field.

In order to make use of (1.114), we must first determine the electron-density distribution. This may be accomplished by solving the diffusion equation

$$D_a \frac{d^2n}{dx^2} + n\nu_i = 0 \quad (1.115)$$

Since the ionization frequency  $\nu_i$  is a function of  $E_e/p$ , the value of  $\nu_i$  will vary with position as long as  $E_e$  is not constant across the gap. Thus to

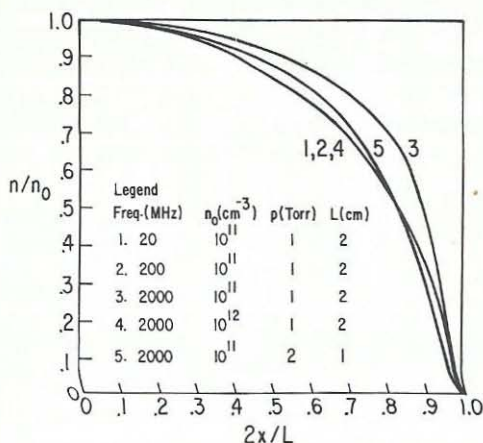


FIGURE 1.21. The spatial distribution of electron density in a helium discharge. Operating conditions for each curve are given in Table 1.2.

determine  $n(x)$  we must consider (1.114) and (1.115) together with experimental data on  $\nu_i/p$  versus  $E_e/p$ .

Solutions for the distributions of electron density and  $E_e/p$  in a helium discharge have been obtained by Bell [37]. These results are illustrated in Figures 1.21 and 1.22. The conditions for each of the curves are given in Table 1.2. For a midplane electron density of  $10^{11} \text{ cm}^{-3}$  it can be observed that

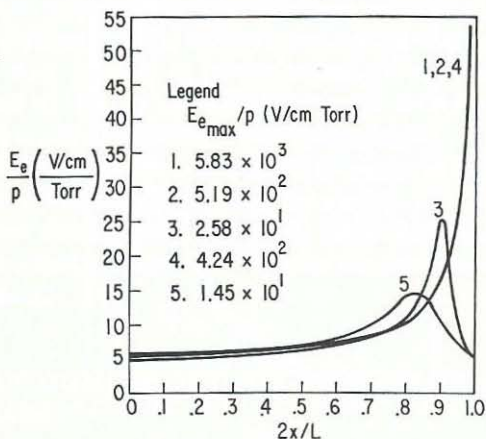


FIGURE 1.22. The spatial distribution of electric field strength in a helium discharge. Operating conditions for each curve are given in Table 1.2.

TABLE 1.2. Operating Conditions for Results Shown in Figs. 1.21, 1.22, and 1.23

$f$ (MHz)	$p$ (torr)	$L$ (cm)	$n_0$ ( $\text{cm}^{-3}$ )	$r$	$\alpha$
20	1	2	$10^{11}$	$2.01 \times 10^4$	20.30
200	1	2	$10^{11}$	$2.01 \times 10^2$	2.03
2000	1	2	$10^{11}$	2.01	0.20
2000	1	2	$10^{12}$	$2.01 \times 10^1$	0.20
2000	2	1	$10^{11}$	2.01	0.40

the curves for  $n^*$  and  $E_e/p$  at 20 and 200 MHz are identical. A noticeable change is produced, however, when the driving frequency is increased to 2000 MHz. Increasing the midplane electron density to  $10^{12} \text{ cm}^{-3}$  causes the solutions to coincide again with those obtained at the lower frequencies.

The observed behavior can be interpreted in terms of (1.114) which governs the magnitude of  $E_e$  as a function of electron density. When  $r \gg \alpha$ , then

$$E_e \simeq E_{e0} \left( \frac{n_0}{n} \right) \quad (1.116)$$

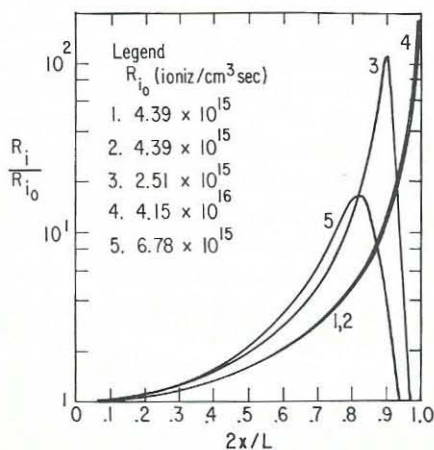


FIGURE 1.23. The spatial distribution of ionization rate in a helium discharge. Operating conditions for each of the curves is given in Table 1.2.

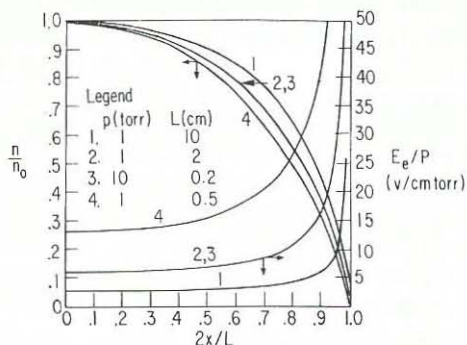


FIGURE 1.24. The spatial distribution of electron density and  $E_e/p$  as a function of pressure and gap length in a helium discharge ( $r \gg \alpha$ ).

except for a very narrow region near  $x^* = 1$ , where  $(r - 1)$  approaches the magnitude of  $\alpha$ . Where (1.116) is valid,  $E_e$  is insensitive to both  $n_0$  and  $\omega$ . By contrast, when  $r \approx \alpha$ , both variables affect the field distribution. Since the local value of  $E_e$  determines the local value of  $\nu_i$ , the relative magnitudes of  $r$  and  $\alpha$  will also influence  $n^*$ .

The effects of operating conditions on the distribution of rates of reaction is illustrated in Figure 1.23. The normalized rate of ionization is plotted as a function of position. As can be seen, the distributions of ionization rates for 20 and 200 MHz are identical. For the same value of  $pL$ , the distribution at 2000 MHz is different and is, furthermore, sensitive to variations in  $p$  and  $L$ , even though their product is held constant. When the midplane electron density is raised to  $10^{12} \text{ cm}^{-3}$ , the distribution of rates for 2000 MHz becomes identical to that observed at the lower frequencies.

Figure 1.24 illustrates the effects of varying  $p$  and  $L$  under the restriction  $r \gg \alpha$ . Both the electron density and the electric field distributions are seen to change when either  $p$  or  $L$  is varied. However, when the product  $pL$  is maintained constant, the two distributions are not affected by the individual values of  $p$  and  $L$ .

## 1.6. PRODUCTION OF ATOMIC OXYGEN IN A MICROWAVE DISCHARGE

The material discussed in the previous sections can now be used to develop a model for the overall kinetics of a reaction occurring in a high-frequency discharge. As an example we shall consider the dissociation of oxygen in a microwave discharge. This system is chosen because of the availability of

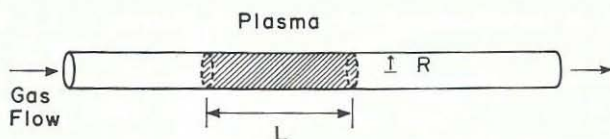
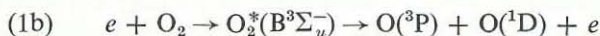


FIGURE 1.25. Schematic of the geometry used for the model of an oxygen discharge.

the necessary physical data and experimental measurements against which the predictions of the model can be tested.

For the model we shall consider the discharge to have the form of a cylindrical plug as shown in Figure 1.25. Within the discharge the electron density and electric field are taken to be constant at the value of the volumetric averages of these quantities. Since we are considering an open system, the gas pressure throughout the discharge tube will be uniform. Consequently, the gas density within the discharge will differ from that elsewhere only if there is a difference in gas temperature.

Dissociation of molecular oxygen can occur by one of two processes involving excitation from the ground state to either the  $A^3\Sigma_u^+$  or the  $B^3\Sigma_u^-$  excited state by electron collision. These reactions can be expressed as



The production of atomic oxygen by dissociative attachment



can be neglected since the reverse of reaction (4) is very rapid ( $k = 3.0 \times 10^{-10}$  cm<sup>3</sup>/sec) and would serve to remove atomic oxygen as quickly as it was formed by reaction (1c). The experimentally determined cross-sections for reactions (1a–1c) have already been illustrated in Section 1.4 (see Fig. 1.10).

In the present model the rate of oxygen dissociation is characterized by the sum of reactions (1a) and (1b). A rate constant can then be determined from the expression

$$k_1 = \sqrt{\frac{8}{\pi m}} (kT_e)^{-3/2} \int_0^\infty \varepsilon \sigma_1(\varepsilon) e^{-\varepsilon/kT_e} d\varepsilon \quad (1.117)$$

where  $T_e$  is the electron temperature,  $m$  is the mass of the electron,  $\varepsilon$  is the electron energy, and  $\sigma_1$  is the total dissociation cross-section. In formulating

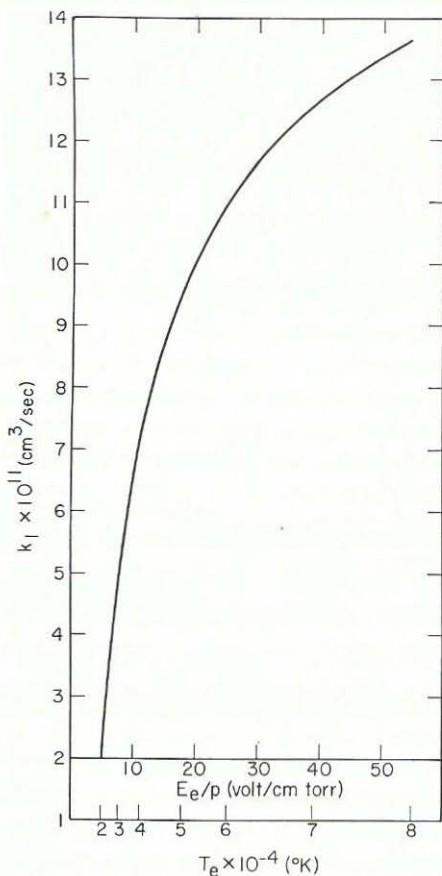
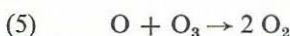


FIGURE 1.26. The rate constant for oxygen dissociation as a function of  $T_e$  and  $E_e/p$ .

(1.117), it has been assumed that the electron-energy distribution function is Maxwellian. A discussion of the suitability of this form of distribution function has been given in Section 1.4. The value of  $k_1$  computed from (1.117) is shown in Figure 1.26 as a function of  $T_e$ . The scale along the abscissa has also been represented in terms of  $E_e/p$ . In making this transformation, Myers' [33] computations of the average electron energy versus  $E_e/p$  have been used together with the relationship  $3/2 kT_e = \langle \epsilon \rangle$ .

Loss of atomic oxygen within the discharge proceeds by both homogeneous and heterogeneous processes. Three separate paths for homogeneous

recombination can be considered:



Rate constants for these reactions are listed in Table 1.1. Heterogeneous recombination of atomic oxygen takes place on the walls of the discharge tube, and the efficiency of this process is characterized by the wall recombination coefficient  $\gamma$ . An experimentally determined value of  $\gamma$  for oxygen recombining on silica is also given in Table 1.1.

If we now consider a differential volume of the reactor, a species balance on atomic oxygen can be expressed as

$$\frac{4FN}{(2N - n_1)^2} \frac{dn_1}{dV} = 2k_1 \langle n_e \rangle (N - n_1) - \frac{1}{2R} n_1 v_r \gamma - 2k_2 n_1^2 (N - n_1) - 2k_3 n_1^3 - 2k_4 n_1 (N - n_1)^2 \quad (1.118)$$

where  $n_1$  is the concentration of atomic oxygen,  $N$  is the total gas concentration,  $\langle n_e \rangle$  is the volume-averaged electron density,  $F$  is the flow rate of molecular oxygen fed to the reaction,  $V$  is the reactor volume,  $R$  is the radius of the discharge tube, and  $v_r$  is the random velocity of oxygen atoms. In formulating (1.125), a one-dimensional plug flow model of the reactor has been assumed. Radial diffusion has been neglected on the basis of a previous analysis [38] of a similar problem which showed that the rate of diffusion of atomic species in a discharge is sufficiently fast to eliminate transverse concentration gradients. Axial diffusion has also been neglected since the ratio  $k_1 \langle n_e \rangle D_{12} / (F/N\pi R^2)^2$  is less than 1 [39] and hence the axial gradients will not be sufficiently high to cause significant axial dispersion.

In order to evaluate the term in (1.118) describing the rate of dissociation, we must first evaluate  $k_1$  and  $\langle n_e \rangle$  for a chosen set of operating conditions. If we describe the operating conditions by the gas pressure  $p$ , the diffusion length  $\Lambda$ , and the power density  $\bar{P}$ , then we have seen that the curves given in Figure 1.19 of Section 1.5 will define the corresponding values of  $E_e/p$  and  $n_e$ . The appropriate value of  $k_1$  may be determined from Figure 1.26.

Equation (1.118) can now be solved by numerical integration in order to determine  $n_1$  for a given set of experimental conditions. The final results are

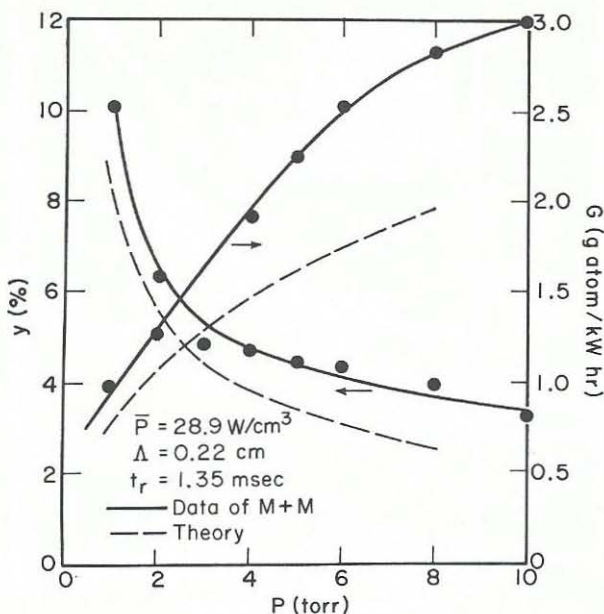


FIGURE 1.27. Conversion and yield versus pressure for reactor A.

then expressed in terms of the conversion  $y$  and the yield  $G$  defined as

$$y = \frac{n_1}{2N - n_1} \quad (1.119)$$

$$G = \frac{7.2 \times 10^6 y F / V}{\bar{P}}$$

A comparison between the predicted values of the conversion and yield and the experimental data of Mearns and Morris [40] is given in Figures 1.27–1.32. In examining these figures it should be noted that two reactors were used in the experimental work. These are referred to as reactor A and reactor B. The type of microwave cavity used with each reactor, the dimensions of the discharge tube, and the approximate discharge volume are listed in Table 1.3.

In Figures 1.27–1.32 the experimental data represent the conversion and yield at the exit from the discharge. Since a direct measurement of these quantities could not be made, Mearns and Morris determined them by back-extrapolating from measurements made downstream from the discharge

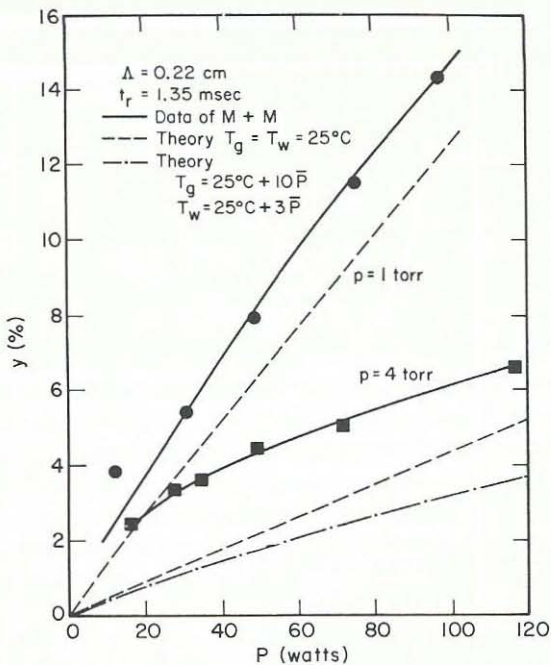


FIGURE 1.28. Conversion versus power for reactor A.

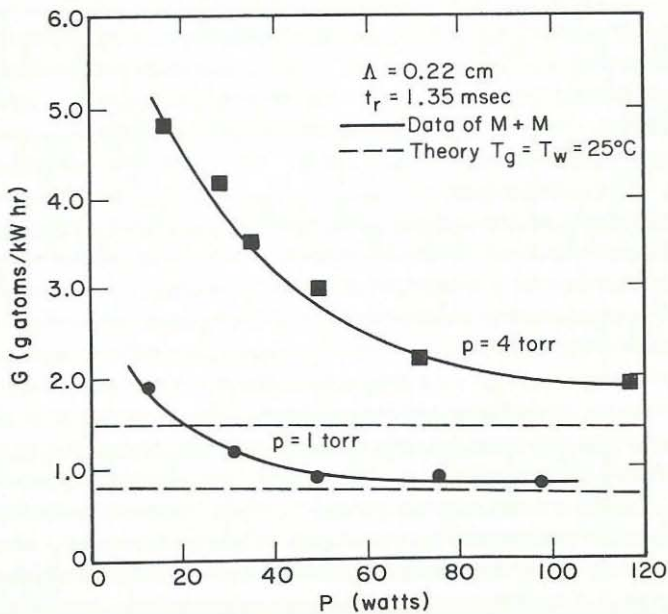


FIGURE 1.29. Yield versus power for reactor A.

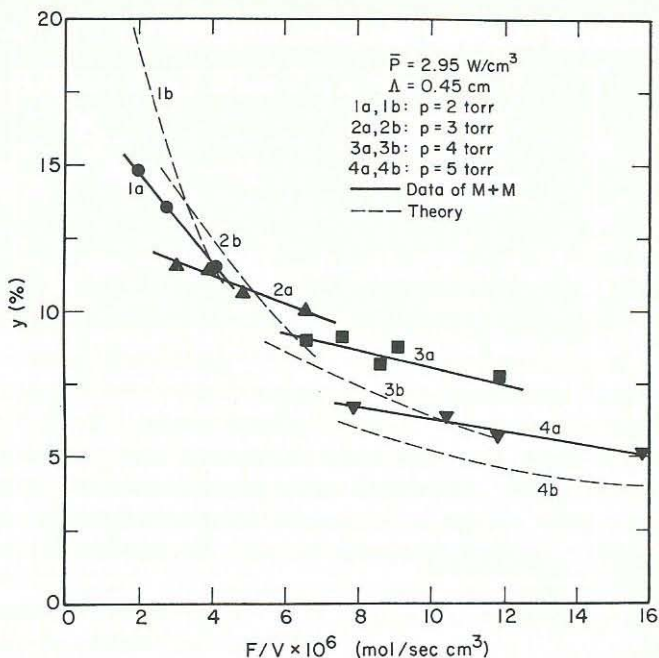


FIGURE 1.30. Conversion versus  $F/V$  for reactor B.

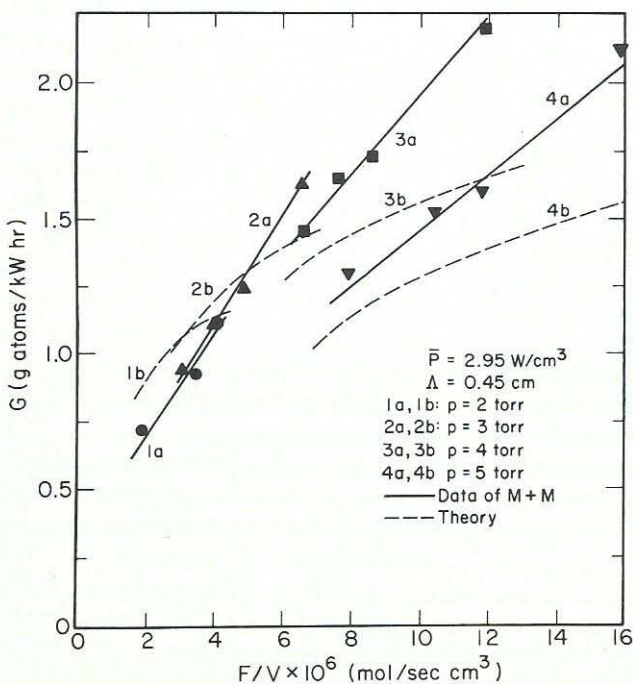


FIGURE 1.31. Yield versus  $F/V$  for reactor B.

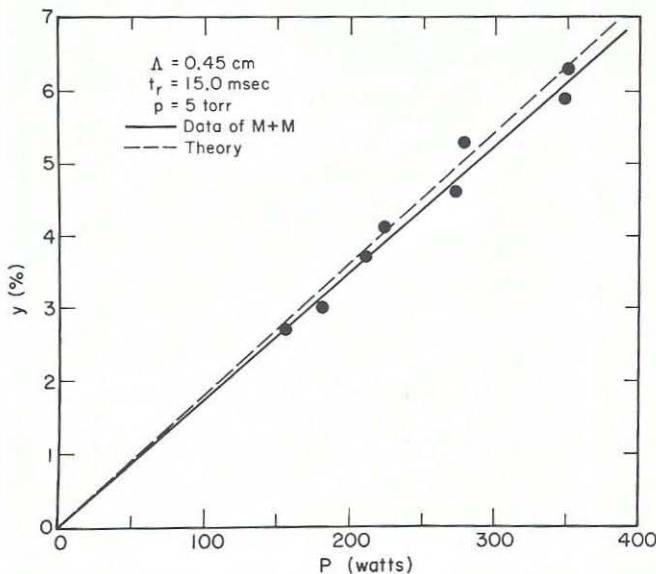


FIGURE 1.32. Conversion versus power for reactor B.

itself. As a result, the experimental points may contain inaccuracies arising from the method and rate constants used to perform the extrapolations. However, it is not possible to evaluate the significance of these inaccuracies.

The response of conversion and yield to increasing pressure is illustrated in Figure 1.27. The experimental results shown there are for reactor A and were obtained for a constant power of 63 W and a residence time of 1.35 msec. The computed curves derived from the model are seen to follow the trends of the data but lie between 20 and 30% lower than the data.

The decrease in conversion with increasing pressure shown in Figure 1.27 results from the superposition of three separate effects which can be elucidated through an examination of (1.118). For this purpose (1.118) is first rewritten

TABLE 1.3. Dimensions of the Reactors Used by Mearns and Morris [40]

Reactor characteristic	Reactor A	Reactor B
Microwave cavity	Coaxial	Cylindrical
Discharge tube <sup>a</sup> radius, $R$	0.53 cm	1.09 cm
Discharge volume	2-3 cm <sup>3</sup>	70 cm <sup>3</sup>

<sup>a</sup> Both discharge tubes were made of silica.

in terms of atomic mole fraction  $x = n_1/N$  as

$$\frac{4F}{N(2-x)^2} \frac{dx}{dV} = 2k_1 \langle n_e \rangle (1-x) - \frac{1}{2R} v_r \gamma x - 2k_2 N^2 x^2 (1-x) - 2k_3 N^2 x^3 - 2k_4 N^2 x (1-x)^2 \quad (1.120)$$

From Figures 1.19 and 1.26 it can be observed that both  $k_1$  and  $\langle n_e \rangle$  decrease as the pressure is increased. This has the effect of reducing the dissociation rate term on the right-hand side of (1.120). The second effect of increased pressure is to cause an increase in the rate of homogeneous recombination of atomic oxygen. Finally one must take into account the increase in  $F$  which is required in order to maintain a constant residence time when the pressure is increased. This change produces a reduction in the conversion by enhancing the convective loss of atomic oxygen.

The effects of power for a fixed pressure and residence time are shown in Figures 1.28 and 1.29. Here again the experimental data are for reactor A. In this case the model predicts a linear rise in conversion with increased power. The experimental data for 1 torr are essentially consistent with this trend but for 4 torr show a less rapid rise in conversion with power. For both pressures the computed conversions are less than the experimental, the maximum deviation being 14% at 1 torr and 54% at 4 torr. The linear relationship between conversion and power predicted by the model is the result of the proportionality between the electron density and power indicated in Figure 1.19. Since the overall conversion for both pressures is relatively low, non-linear effects due to homogeneous recombination cannot be observed.

The calculations shown in Figures 1.28 and 1.29 were performed under the assumption that the temperature of the gas and the discharge tube wall remained at 25°C independent of the power dissipated. In order to explore the effects of variations in these temperatures, calculations were performed under the assumption that the gas temperature increased at the rate of 10°C cm<sup>3</sup>/W and the wall temperature at the rate of 3°C cm<sup>3</sup>/W. An examination of (1.119) or (1.120) shows that, for a fixed gas pressure, five quantities will respond to a variation in the gas temperature,  $N$ ,  $k_1$ ,  $\langle n_e \rangle$ ,  $v_r$ , and  $k_4$ . The reduction of gas density with increasing temperature leads to a decrease in the value of  $p\Lambda$  which in turn causes  $k_1$  and  $\langle n_e \rangle$  to increase. The increase in the random velocity enhances the rate of heterogeneous recombination by increasing the flux of atomic oxygen to the wall of the discharge tube. The increase in the discharge tube wall temperature affects only  $\gamma$  which for a silica tube has been shown to vary from  $1.6 \times 10^{-4}$  at 20°C to  $1.4 \times 10^{-2}$  at 600°C [30].

Figure 1.29 illustrates the predicted values of the conversion for 4 torr when both the gas and discharge tube wall temperatures are taken to increase with power. As can be seen, the conversions computed for the elevated temperatures lie below those computed for  $T_g = T_w = 25^\circ\text{C}$ . These results can be explained as follows. With the increase in gas temperature, both  $k_1$  and  $\langle n_e \rangle$  increase; however, the product  $k_1 \langle n_e \rangle N$  decreases due to the inverse dependence of  $N$  on the gas temperature. On the other hand, the heterogeneous rate of recombination increases with power due to the increases in both  $v_r$  and  $\gamma$ . This latter effect is only partially offset by the reduction in the rate of reaction (4) due to the decrease in  $k_4$ . Thus, for a given power, the effect of assuming an increase in  $T_g$  and  $T_w$  is to cause the rate of dissociation to decrease and rate of recombination to increase, both of which lead to a reduction in the conversion.

The effects of pressure and flow rate on the conversion and yield obtained from reactor B are illustrated in Figures 1.30 and 1.31. For each pressure the curve of predicted conversion intersects the curve drawn through the data and exhibits a more rapid decrease with flow rate than shown by the data. The maximum deviations between the calculated and measured conversions occur at 2 torr where they reach a level of 22%. As the pressure is increased, the slopes of the pairs of curves approach each other more and more closely. Similar patterns can be observed in the curves representing yield versus  $F/V$ . The most likely source of error in these computations is an overestimation of  $k_1$  at the lower pressures. The assumption of a smaller value of  $k_1$  would lead to a more gradual decline in conversion with flow rate and would improve the fit to the data.

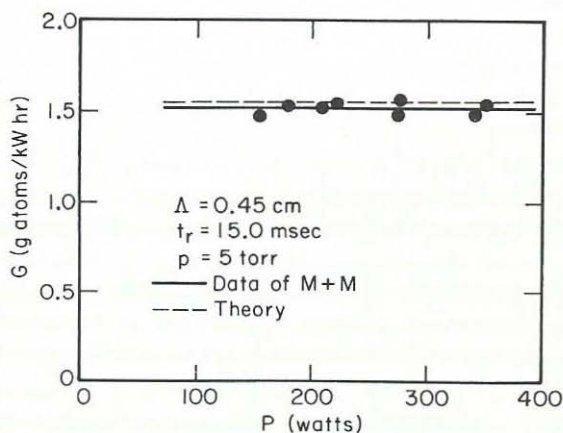


FIGURE 1.33. Conversion versus power for reactor B.

The effect of power on the conversion and yield obtained from reactor B are shown in Figures 1.32 and 1.33. Both the experimental and the computed conversions illustrate a linear dependence on power. The nearly perfect agreement between theory and experiment shown in Figures 1.32 and 1.33 may be misleading since the effects of increased gas and discharge tube wall temperature have not been taken into account. It should be noted, however, that the introduction of these effects should not produce significant variations in the results because the power densities corresponding to the conditions in Figures 1.32 and 1.33 are quite low, e.g., 0–6 W/cm<sup>3</sup>.

### REFERENCES

- [1] W. P. ALLIS, "Motion of Ions and Electrons," in *Handbuch der Physik*, Vol. 21, Springer-Verlag, Berlin, 1956, p. 383.
- [2] H. DREICER, *Phys. Rev.* **117**, 343 (1960).
- [3] H. MARGENAU, *Phys. Rev.* **73**, 309 (1948).
- [4] A. VON ENGEL, *Ionized Gases*, Oxford Press, New York, 1955.
- [5] E. W. MCDANIEL, *Collision Phenomena in Ionized Gases*, Wiley, New York, 1964.
- [6] H. S. W. MASSEY, E. H. S. BURHOP, and H. B. GILBODY, *Electronic and Ionic Impact Phenomena*, Oxford Press, New York, 1971.
- [7] W. P. ALLIS and D. J. ROSE, *Phys. Rev.* **93**, 84 (1954).
- [8] E. W. MCDANIEL, V. CERMAK, A. DALGARNO, E. E. FERGUSON, and L. FRIEDMAN, *Ion-Molecule Reactions*, Wiley-Interscience, New York, 1970.
- [9] D. RAPP and P. ENGLANDER-GOLDEN, *J. Chem. Phys.* **43**, 1464 (1965).
- [10] E. W. ROTHE, L. L. MARINO, R. H. NEYNABER, and S. M. TRUJILLO, *Phys. Rev.* **125**, 582 (1962).
- [11] D. RAPP, P. ENGLANDER-GOLDEN, and D. D. BRIGLIA, *J. Chem. Phys.* **42**, 4081 (1965).
- [12] D. RAPP and D. D. BRIGLIA, *J. Chem. Phys.* **43**, 1480 (1965).
- [13] H. MYERS, *J. Phys. B* **2**, 393 (1969).
- [14] F. C. FEHSENFELD, E. E. FERGUSON, and A. L. SCHMELTEKOPF, *Planet. Space Sci.* **13**, 579 (1965).
- [15] R. F. STEBBINGS, A. C. H. SMITH, and H. B. GILBODY, *Phys. Rev.* **38**, 2280 (1963).
- [16] J. J. LEVENTHAL and L. FRIEDMAN, *J. Chem. Phys.* **46**, 997 (1967).
- [17] D. A. DURDEN, P. KEARLE, and A. GOOD, *J. Chem. Phys.* **50**, 805 (1969).
- [18] R. M. SNUGGS, D. J. VOLZ, J. H. SCHUMMERS, R. D. LASER, I. R. GATLAND, D. W. MARTIN, and E. W. MCDANIEL, Technical Report, School of Physics, Georgia Institute of Technology, Atlanta, Ga. March 29, 1970.

## 56 FUNDAMENTALS OF PLASMA CHEMISTRY

- [19] E. E. FERGUSON, F. C. FEHSENFELD, and A. L. SCHMELTEKOPF, *Adv. Chem. Ser.* **80**, 83 (1969).
- [20] F. C. FEHSENFELD, E. E. FERGUSON, and A. L. SCHMELTEKOPF, *J. Chem. Phys.* **45**, 1844 (1966).
- [21] B. R. TURNER, D. M. J. COMPTON, and J. W. MCGOWAN (eds.), General Atomics Report G.A. 7419 (1966).
- [22] L. G. MCKNIGHT and J. M. SAWINA, DASA Conference, Palo Alto, Ca., (June 1969).
- [23] F. C. FEHSENFELD, E. E. FERGUSON, and D. K. BOHME, *Planet. Space Sci.* **17**, 1759 (1970).
- [24] T. L. BAILEY and P. MAHADEVAN, *J. Chem. Phys.* **52**, 179 (1969).
- [25] F. C. FEHSENFELD, D. L. ALBRITTON, J. A. BURT, and H. I. SCHIFF, *Can. J. Chem.* **47**, 1793 (1969).
- [26] S. C. BROWN, *Basic Data of Plasma Physics, 1966*, M.I.T. Press, Cambridge, Mass., 1967, p. 213.
- [27] W. H. ABERTH and J. R. PETERSON, *Phys. Rev.* **1**, 158 (1970); R. E. OLSON, J. R. PETERSON, and J. MOSELEY, *J. Chem. Phys.* **53**, 3391 (1970).
- [28] K. SCHOFIELD, *Planet. Space Sci.* **15**, 643 (1967).
- [29] H. S. JOHNSTON, "Gas Phase Reaction Kinetics of Neutral Oxygen Species," *Nat. Stand. Ref. Data Ser., Nat. Bur. Stand. NSRDS-NBS 20* (1968).
- [30] J. C. GREAVES and J. W. LINNETT, *Trans. Farad. Soc.* **55**, 1355 (1959).
- [31] E. GERJUOY and S. STEIN, *Phys. Rev.* **97**, 1671 (1955).
- [32] R. D. HAKE and A. V. PHELPS, *Phys. Rev.* **158**, 70 (1967).
- [33] H. MYERS, *J. Phys. B* **2**, 393 (1969).
- [34] H. SABADIL, *Beitr. Plasma Phy.* **53** (1971).
- [35] S. C. BROWN, *Introduction to Electrical Discharges in Gases*, Wiley, New York, 1966.
- [36] D. J. ROSE and S. C. BROWN, *Phys. Rev.* **85**, 310 (1955).
- [37] A. T. BELL, *I&EC Fund. Quart.* **9**, 160, 679 (1970).
- [38] A. T. BELL, *I&EC Fund. Quart.* **11**, 209 (1972).
- [39] E. E. PETERSEN, *Chemical Reaction Analysis*, Prentice-Hall, Englewood Cliffs, N.J., 1965.
- [40] A. M. MEARNS and A. J. MORRIS, *CEP Symp. Series* **112**, 37 (1971).